1 **A Range of Outcomes: The Combined Effects of Internal Variability and Anthropogenic**

2 **Forcing on Regional Climate Trends over Europe**

4 Clara Deser* and Adam S. Phillips

5 National Center for Atmospheric Research, Boulder CO USA

7 *EGU Nonlinear Processes in Geophysics Special Issue*

8 "Interdisciplinary perspectives on climate sciences – highlighting past and current scientific

9 achievements"

11 Submitted October 14, 2022

12 Revised December 26, 2022

15 * Corresponding author: Clara Deser cdeser@ucar.edu

17   **Abstract**

18   Disentangling the effects of internal variability and anthropogenic forcing on regional climate

19   trends remains a key challenge with far-reaching implications. Due to its largely unpredictable

20   nature on timescales longer than a decade, internal climate variability limits the accuracy of climate

21   model projections, introduces challenges in attributing past climate changes, and complicates

22   climate model evaluation. Here, we highlight recent advances in climate modeling and physical

23   understanding that have led to novel insights on these key issues. In particular, we synthesize new

24   findings from Large Ensemble simulations with Earth System Models, Observational Large

25   Ensembles, and "dynamical adjustment" methodologies, with a focus on European climate.

27   **1. Introduction**

28   *a. Internal variability and forced climate change*

29   The climate system is highly variable in both space and time. This variability originates from

30   processes within the coupled ocean-atmosphere-cryosphere-land-biosphere system, as well as

31   from external influences such as solar and orbital cycles, volcanic eruptions, and anthropogenic

32   emissions of greenhouse gases and sulfate aerosols. A primary source of internally-generated

33   variability is the atmospheric general circulation, which produces familiar day-to-day and week-

34   to-week weather fluctuations. The non-linear nature of atmospheric dynamics limits predictability

35   to less than a few weeks; beyond this time scale, atmospheric motions may be considered as

36   random stochastic processes, often termed "weather noise" (e.g., Lorenz, 1963; Leith, 1973; James

37   and James, 1992). It is important to note that such "weather noise" imparts variability on a

38   continuum of time scales, from sub-monthly to decadal and longer (e.g., Madden, 1975; Deser et

39   al. 2012; Thompson et al. 2015).

41 Another important source of internally-generated variability is the coupling between the ocean and

42 atmosphere. Large-scale air-sea interactions give rise to distinctive patterns (or "modes") of

43 variability on interannual and longer time scales, including phenomena such as "El Niño –

44 Southern Oscillation" (ENSO; Wang et al. 2017), "Pacific Decadal Variability" (PDV; Newman

45 et al. 2016) and "Atlantic Multi-decadal Variability" (AMV; Zhang et al. 2019). Like the

46 atmospheric general circulation, these coupled modes are governed by non-linear dynamical

47 processes which limit their predictability. For example, forecast skill is generally limited to 1-2

48 years for ENSO (Jin et al., 2008; DiNezio et al. 2017; Wu et al. 2021), 5 years for PDV (Teng and

49 Branstator, 2010; Meehl et al., 2016; Gordon and Barnes, 2022) and 10 years for AMV (Griffies

50 and Bryan, 1997; Trenary and DelSole, 2016; Yeager et al., 2018). Beyond these predictability

51 time horizons, internally-generated variability can be thought of as a "roll of the dice", introducing

52 unavoidable uncertainty to climate model projections especially at local and regional scales (e.g.,

53 Deser et al. 2012, 2014 and 2020a).

55 Not only does unpredictable internal variability cause irreducible uncertainty in future climate

56 projections, it also confounds interpretation of the historical climate record. For example, internal

57 variability may partially obscure the regional climate response to external forcings including

58 industrial greenhouse gas emissions, stratospheric ozone depletion and volcanic eruptions

59 (Wallace et al., 2013; Schneider et al. 2015; Lehner et al. 2016; McGraw et al. 2016). In some

60 areas, climate trends driven by internal processes may even outweigh those due to anthropogenic

61 influences over the past 30-60 years (Deser et al., 2012, 2016 and 2017; Wallace et al., 2013; Swart

62 et al. 2015; Lehner et al. 2017). It is important to note that such internally-generated multi-decadal

63   trends need not originate from slow processes within the ocean or coupled ocean-atmosphere

64   system: indeed, random fluctuations of the atmospheric circulation independent of oceanic

65   influences have been shown to drive a large fraction of long-term precipitation and temperature

66   trends over North America and Eurasia (Deser et al. 2012; McKinnon and Deser, 2018). The co-

67   existence of internal and anthropogenic factors necessitates a probabilistic approach to detection

68   and attribution of the human contribution to extreme weather events.

69

70   The prevalence of internal climate variability also complicates model evaluation efforts, since the

71   simulated temporal sequence of (unpredictable) internal variability need not match observations

72   even if the model's physics are realistic. Further, the brevity of the instrumental record provides

73   only a limited sampling of internal variability, hindering robust model evaluation. Thus, climate

74   models may show an apparent bias with respect to observations, but this could be entirely

75   attributable to sampling issues rather than indicative of a true bias due to incorrect model physics.

76   Apparent model bias due to sampling uncertainty must be kept in mind when assessing fidelity of

77   simulated modes of internal variability (e.g., Wittenberg et al. 2009; Deser et al. 2017; Capotondi

78   et al. 2020; Fasullo et al. 2021; McKenna and Maycock, 2021), transient climate sensitivity (Dong

79   et al. 2021; Andrews et al. 2022), and "signal-to-noise" properties of initial-value predictions and

80   forced responses (e.g., Scaife and Smith, 2018; Smith et al., 2020; Klavans et al. 2021). In

81   particular, even with 100 years of data, sampling uncertainty is a limiting factor for evaluating

82   ENSO properties in climate models, including its global atmospheric teleconnections and

83   associated climate impacts (Deser et al. 2017 and 2018; Capotondi et al. 2020) and forced changes

84   thereof (Stevenson et al. 2012; Maher et al. 2018; Maher et al. 2022; O'Brien and Deser, 2022).

85   This issue is particularly acute for model assessment of modes of decadal variability such as PDV

86   and AMV due to the paucity of samples in the short instrumental record (Deser and Phillips 2021;

87   Fasullo et al. 2021).

88

89   *b. Initial-condition Large Ensemble Simulations with Earth System Models*

90   To overcome the issue of sampling uncertainty, a recent thrust in climate modeling is to run a large

91   number of simulations (30-100) with the same coupled model and the same radiative forcing

92   protocol (historical and/or future scenario) but vary the initial conditions. The initial-condition

93   variation can be accomplished by introducing a random perturbation to the atmosphere on the order

94   of the model's numerical round-off error (e.g., 10^{-14} K in the case of atmospheric temperatures;

95   Kay et al. 2015) or it can be done by selecting a different ocean state from a long control run of

96   the coupled model, or a combination of the two (Deser et al. 2020a and Rodgers et al. 2021).

97   Regardless of the method used, the initial-condition perturbation serves to create ensemble spread

98   once the memory of the initial state is lost, typically within a month for the atmosphere and a few

99   years to a couple of decades for the ocean (Yeager et al., 2018). The ensuing ensemble spread is

100 thus solely attributable to random internal variability (e.g., the "butterfly effect" in chaos theory);

101 see Lorenz (1963) and Tel et al. (2019). Because the temporal sequences of internal variability

102 unfold differently in the various ensemble members once the memory of the initial conditions is

103 lost, one can estimate the forced component at each time step (at each location) by averaging the

104 members together, provided the ensemble size is sufficiently large. The internal component in each

105 ensemble member is then obtained as a residual from the ensemble-mean. Note that a larger

106 ensemble may be needed for some aspects of the forced response than others, depending on the

107 relative magnitudes of the forced response and internal variability (Milinski et al., 2020). For

108 example, forced changes in ocean heat content may be readily detected with just a few members

109   (Fasullo and Nerem, 2018), while forced changes in atmospheric circulation (Deser et al., 2012)

110   or precipitation and temperature extremes (Tebaldi et al. 2021) may require 20-30 members.

111   Detecting forced changes in the characteristics of internal variability itself, such as its amplitude,

112   spatial pattern and remote teleconnections, may necessitate even larger ensembles (Milinski et al.,

113   2020; Bódai et al., 2020; Bódai et al., 2022; O'Brien and Deser, 2023).

114

115   Initial-condition Large Ensembles (LEs for short) have proven enormously useful for separating

116   internal variability and forced climate change on regional scales in models, and for providing

117   robust sampling of models' internal variability by pooling together all of the ensemble members

118   (e.g., Deser et al., 2012; Kay et al., 2015; Maher et al., 2019; Deser et al. 2020a; Lehner et al.,

119   2020). They have also been used to assess externally-forced changes in the characteristics of

120   simulated internal variability, including extreme events for which large sample sizes are crucial

121   (e.g., Tebaldi et al., 2021; O'Brien and Deser, 2023). Additionally, they have served as

122   methodological testbeds for evaluating approaches to detection and attribution of anthropogenic

123   climate change in the (single) observational record (e.g., Deser et al., 2016; Barnes et al., 2019;

124   Sippel et al., 2019 and 2021; Santer et al. 2019; Bonfils et al., 2019; Wills et al., 2020). Until the

125   advent of LEs, it was problematic to identify the sources of model differences in the Coupled

126   Model Intercomparison Project (CMIP) archives due to the limited number of simulations

127   (generally < 3) for each model (i.e., structural uncertainty was confounded with uncertainty due to

128   internal variability). This concern has been largely alleviated thanks to the recent availability of

129   LEs with multiple earth system models (e.g., Deser et al. 2020a; Lehner et al., 2020).

130

131   *c. Observationally-based Large Ensemble*

132   Just as in a model LE, the sequence of internal variability in the real world could have unfolded

133   differently. That is, the observational record traces only one of many possible climate histories that

134   could have happened under the same external radiative forcing. For example, El Niño and La Niña

135   events could have occurred in a different set of years, and positive or negative regimes of PDV

136   and AMV could have taken place in different decades. This concept of alternate chronologies,

137   sometimes referred to as the "Theory of Parallel Climate Realizations" (Tel et al., 2019) or the

138   notion of "Contingency" (Gould, 1989), has major implications that call for a reframing of

139   perspective. For example, it means that a single model simulation of the historical period need not

140   match the observed record, even if the model is "perfect" in its physical representation of the real

141   world's climate. However, the statistical characteristics of the model's internal variability must

142   agree with those of the real world, taking into account sampling uncertainty (uncertainty due to

143   limited sampling in the short observational record). Thus, while a single ensemble member need

144   not match observations, the ensemble as a whole should encompass the instrumental data, provided

145   there are enough members to adequately span the range of possible sequences of internal variability

146   (Suarez-Guttierez et al. 2021).

147

148   Another implication of the concept of "parallel climate realizations" is that the climate trends we

149   have experienced are not the only ones that could have occurred under the same radiative forcing

150   conditions. In analogy with a model LE, the observational record is just one "member" of a larger

151   set of possible "members", each with a different (and largely unpredictable) chronology of internal

152   variability. Although one cannot replay the "tape of history", one can construct an "Observational

153   LE" by generating alternate synthetic sequences of internal variability from the instrumental data.

154   Conceptually, this involves removing an estimate of the forced component from the data and then

155   randomizing the residual (internal) variability in time. Importantly, the randomization procedure

156   must be done in a way that preserves the statistical properties of the observed variability including

157   its variance, temporal autocorrelation, and spatial patterns. The resulting synthetic sequences of

158   internal variability derived from the observational record can then be added back to the time-

159   evolving forced response obtained from a climate model LE.

160

161   The development of statistically-based Observational LEs is just beginning, with recent efforts

162   targeting surface climate fields (McKinnon et al., 2017; McKinnon and Deser, 2018 and 2021) and

163   carbon dioxide fluxes across the air-sea interface (Olivarez et al. 2022). Here, we focus on the

164   work of McKinnon and Deser (2018 and 2021) who constructed an Observational LE for global

165   sea level pressure (SLP) and terrestrial precipitation and temperature based on ~100 years of

166   monthly gridded instrumental data. To test the skill of their method, they applied it independently

167   to each member of a climate model LE and then compared the results to the "true" statistical

168   properties of the model's internal variability based on the full set of ensemble members. According

169   to this test, their approach was found to be accurate to within 10-20% at most locations. They then

170   constructed a large (1000 member) ensemble of plausible "parallel worlds" of what the

171   observational record might have looked like had a different sequence of internal variability

172   unfolded by chance. Their Observational LE has been used for many applications, including

173   evaluation of internal variability in climate model LEs, assessment of uncertainty in observed 50-

174   year climate trends, and quantification of extreme precipitation risk over the Upper Colorado River

175   basin, a critical water resource for the western US (McKinnon and Deser 2018 and 2021).

176

177   *d. Dynamical Adjustment*

178   Determining the forced contribution to observed changes in climate remains an ongoing challenge.

179   Most "Detection and Attribution" methods rely on climate models to provide a set of spatial and

180   temporal "fingerprints" of forced climate change that are distinct from patterns of internal

181   variability (Hegerl et al. 2007; Santer et al. 2019; Sippel et al. 2019). These model-based

182   "fingerprints" are then used to assess the proportion of observed climate change that is due to

183   external forcing. However, model shortcomings may limit the accuracy of such methods. Thus, it

184   is also desirable to develop complementary approaches to attribution that do not rely on climate

185   model information. Two such methods, Linear Inverse Modeling (Newman, 2007) and Low-

186   Frequency Pattern Analysis (Wills et al. 2020), leverage the assumption that forced climate change

187   evolves slowly compared to the time scales of internal variability. However, decadal shifts in

188   regional anthropogenic aerosol emissions (Deser et al. 2020b; Persad et al. 2018), in addition to

189   decadal changes in solar and volcanic activity and the rate of greenhouse gas rise, present

190   challenges to this assumption and may complicate interpretation of the results.

191

192   A complementary, physically-based approach to isolating the externally-forced response in

193   observations without reliance on climate model information is the technique of "Dynamical

194   Adjustment". This method aims to remove the influence of atmospheric circulation variability

195   from observed temperature and precipitation data, thereby revealing the thermodynamically-

196   induced component of observed climate change (Wallace et al. 2013; Smoliak et al. 2015; Deser

197   et al. 2016; Guo et al. 2019). According to the current generation of coupled climate models, the

198   forced component of extra-tropical atmospheric circulation changes is small relative to internal

199   variability (Deser et al. 2012; Shepherd, 2014). If models are correct in this regard, then dynamical

200   adjustment can be used to parse the relative contributions of internal dynamics and forced

201 thermodynamics to observed climate changes at middle and high latitudes (Wallace et al. 2013;

202 Deser et al. 2016). A variety of dynamical adjustment algorithms have been developed and tested

203 within the framework of a model LE (Deser et al., 2016; Lehner et al., 2017 and 2018; Smoliak

204 et al., 2015; Guo et al. 2019; Merrifield et al., 2017; Terray 2021; Sippel et al. 2019). These

205 protocols are all based on statistical associations between patterns of SLP and temperature or

206 precipitation deduced from long observational records. Generally, the data are high-pass filtered

207 or detrended so as to avoid aliasing any potential forced component onto the statistical

208 relationships. These procedures generally work best for large-amplitude SLP anomaly patterns,

209 and are more effective for temperature than precipitation due to higher levels of noise in the latter

210 (Guo et al. 2019).

211

212 **2. Data and Methods**

213 We make use of a state-of-the-art 100-member LE conducted with the National Center for

214 Atmospheric Research (NCAR) Community Earth System Model version 2 (CESM2), described

215 in Rodgers et al. (2021). This publicly available LE resource is unprecedented for its combination

216 of large ensemble size, high spatial resolution (approximately 1° in both latitude and longitude),

217 and length of simulation (1850-2100). Each ensemble member is driven by the same radiative

218 forcing scenario (historical from 1850-2014, and SSP3-7.0 from 2015-2100), but begins from a

219 different state on 1 January 1850, taken from a long pre-industrial control simulation. We analyze

220 linear trends in air temperature, precipitation and sea level pressure over the past 50 years (1972-

221 2021) and projected for the next 50 years (2022-2071). It should be noted that memory of the

222 initial state is negligible by the middle of the 20th century for the quantities we analyze; thus,

223   diversity in trends amongst the individual ensemble members is solely due to different random

224   samples of internal variability, which are superimposed upon a common forced response.

225

226   For consistency with the 100-member CESM2 LE, we make use of the first 100 members of the

227   Observational LE (OBS LE) constructed by McKinnon and Deser (2018) to illustrate the diversity

228   of past 50-year trends consistent with the statistical spatio-temporal properties of internal

229   variability in the observational record. For the purpose of comparing directly to the CESM2 LE,

230   we have added the model's forced trend to the internal trend of each OBS LE member. The OBS

231   LE is based on the Berkeley Earth Surface Temperature (BEST) dataset (Rohde et al. 2013), the

232   Global Precipitation Climatology Centre (GPCC) dataset (Schneider et al. 2008), and the

233   Twentieth Century Reanalysis version 2c (20CR) sea level pressure (SLP) dataset (Compo et al.

234   2011).

235

236   We apply the dynamical adjustment methodology of Deser et al. (2016) based on SLP "constructed

237   circulation analogues" to monthly temperature and precipitation during 1900-2021, using the same

238   observational data sets as in the OBS LE. The reader is referred to Deser et al. (2016) for details

239   of the methodology, and to Lehner et al. (2017 and 2018), Guo et al. (2019) and Terray (2021) for

240   additional applications.

241

242   For each ensemble member of the CESM2 and OBS LEs, we form monthly anomalies by

243   subtracting the long-term means for each month individually, and then form seasonal averages

244   (December-February) of the monthly anomalies. We compute 50-year trends of the wintertime

245   anomalies using linear least-squares regression analysis. All results shown in this study are

246   original findings.

247

248   **3. European climate trends**

249   We begin by illustrating the diversity of winter temperature and precipitation trends over Europe

250   during the past 50 years (1972-2021) in the CESM2 and OBS LEs (Sections 3a and b) and

251   projected for the next 50 years (2022-2071) in the CESM2 LE (Section 3c). We then provide a

252   more quantitative view of the relative contributions of forced climate change and internal

253   variability to past and future climate trends using a variety of signal-to-noise metrics, with

254   comparison between the CESM2 and OBS LEs (Section 3d). We summarize the CESM2 LE

255   results by showing the "expected range" of trend outcomes in Section 3e. Finally, we apply the

256   technique of "dynamical adjustment" to estimate the forced component of observed temperature

257   trends (Section 3f), and then use this estimate in conjunction with the OBS LE to produce a purely

258   observational estimate of the plausible range of temperature trend outcomes over the past 60 years

259   (Section 3g).

260

261   *a. Past trends (1972-2021) in the CESM2 LE*

262   The CESM2 model simulates a wide range of wintertime temperature trend patterns for the past

263   50 years due to the combined effects of internal variability and forced response, as illustrated by

264   the first 28 members of the LE (Fig. 1). Recall that the only reason that these trend maps are not

265   identical is because of random differences in internal variability between the members. While

266   moderate warming is seen over most of the European continent in the majority of cases, as

267   expected, some members show regions of considerably greater temperature increase (in excess of

268   1°C per decade for example members 1, 10 and 18), while others exhibit weak cooling in some

269   locations (for example, members 17, 23 and 26; Fig. 1). The relative contributions of internal

270   variability and forced response can be readily discerned by comparing the individual member

271   trends with the ensemble-mean trend (see "EM" panel in Fig. 1). The observed trend ("OBS"

272   panel in Fig. 1) bears a close resemblance to the model's forced trend in both amplitude and spatial

273   pattern. This correspondence may be coincidental, as individual members of the CESM2 LE also

274   resemble the forced response (for example, members 6 and 21), or it may suggest that the model

275   overestimates the amplitude of internally-generated 50-year trends relative to forced trends. The

276   OBS LE results shown below will shed some light on these two possibilities.

CESM2 large ensemble: Temperature trends 1972-2021

277
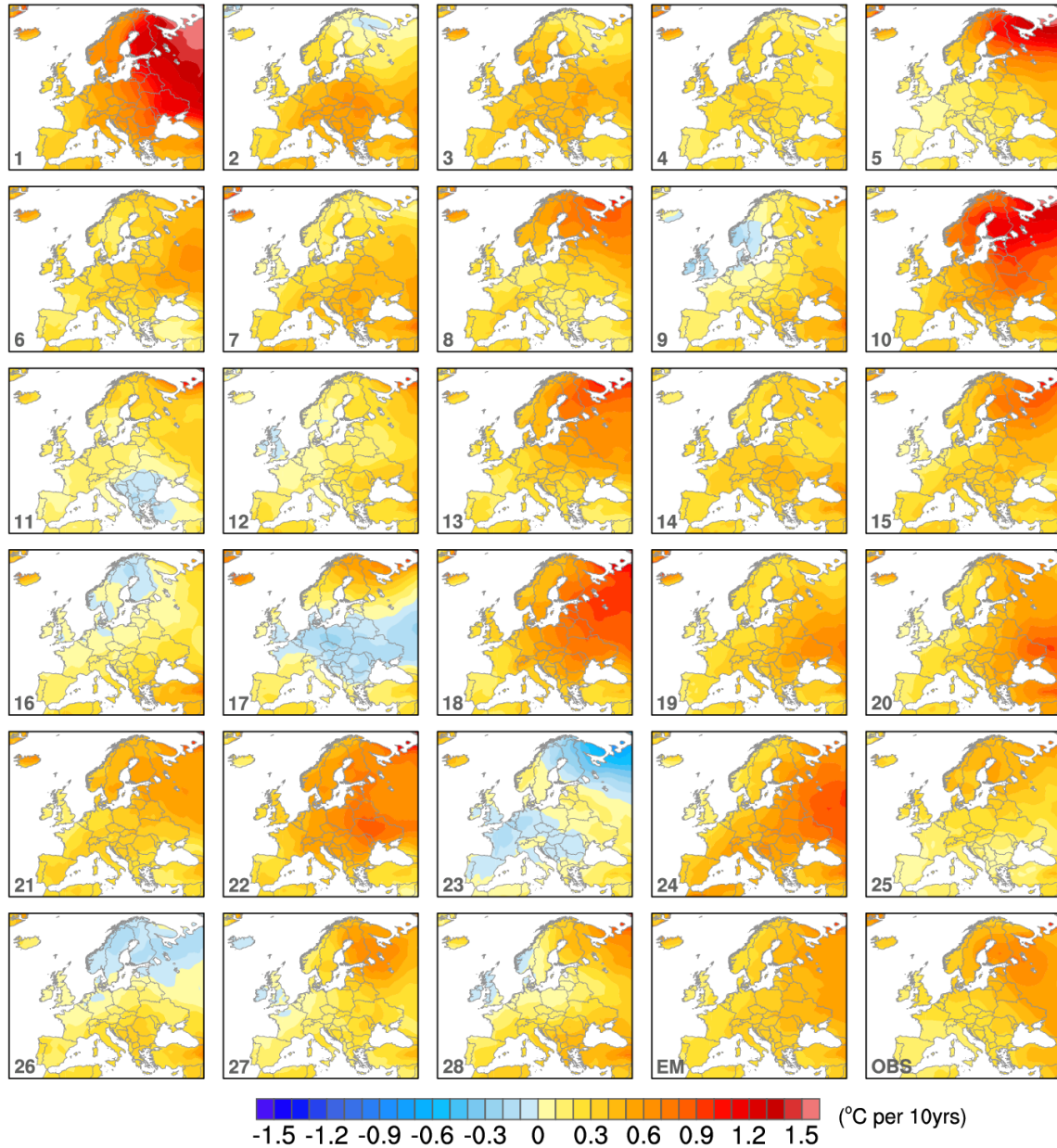
Figure 1. Winter air temperature trends (°C per decade) for the period 1972-2021 as simulated by the first 28 members of the CESM2 Large Ensemble (number in the lower left of each panel denotes the ensemble member) and the 100-member ensemble-mean (panel labeled "EM"). Observed trends are shown in the lower right (panel labeled "OBS").

282
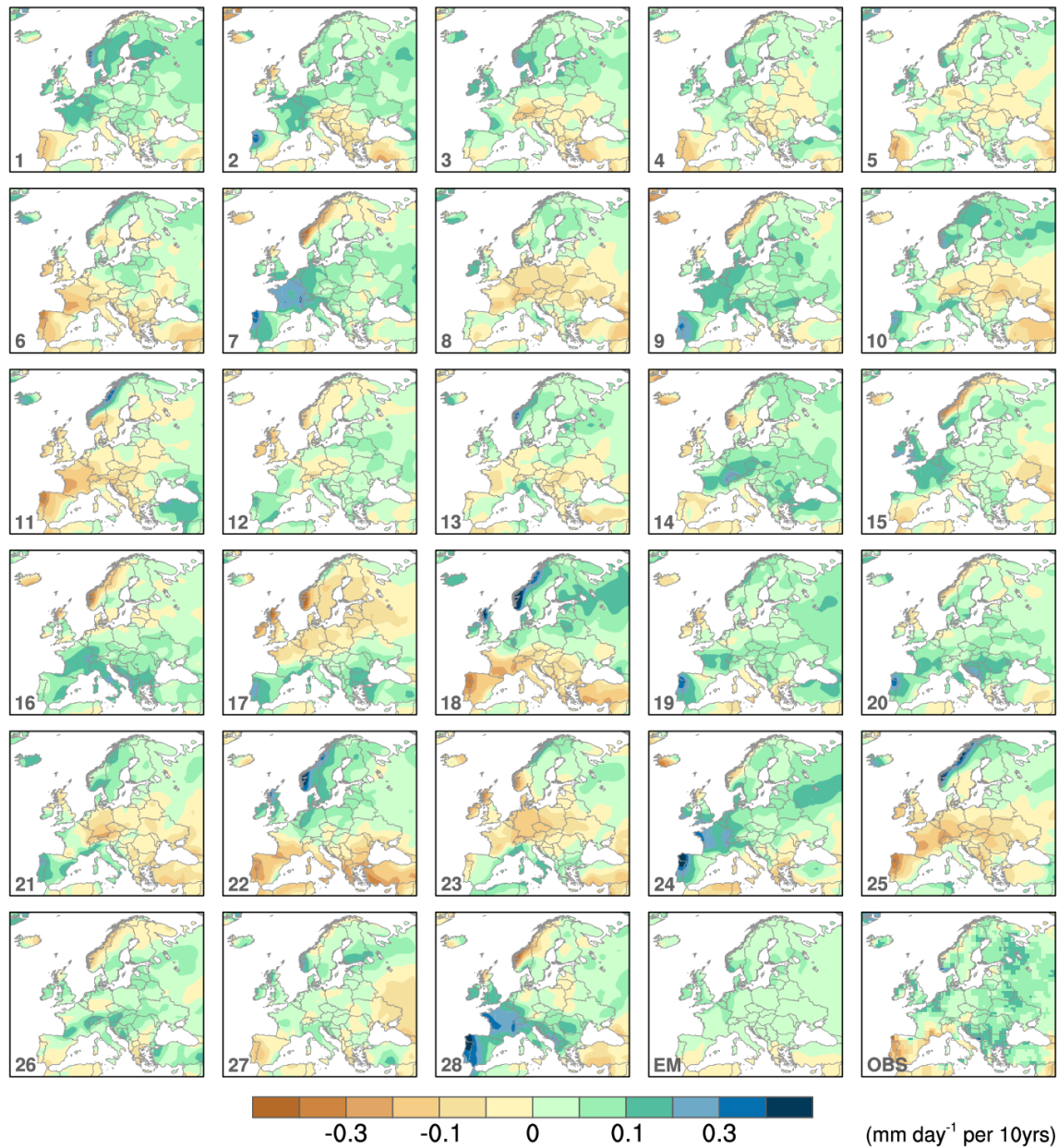
Figure 2. As in Fig. 1 but for precipitation (mm d-1 per decade).

Like temperature, precipitation trends also vary considerably across ensemble members (Fig. 2). While the ensemble-mean trend shows modest increases in precipitation throughout Europe (except for the southernmost fringes), internal variability can evidently overwhelm the forced response in individual simulations. For example, some members show drying over large parts of

290   the continent, while others depict enhanced wetting in the same regions (compare, for example,

291   members 22 and 28, which show nearly opposite patterns). Observed precipitation trends are

292   generally positive, except over Spain, Portugal, southern France and other parts of the western

293   Mediterranean (Fig. 2). The observed precipitation increases, while of the same sign as the

294   model's forced response, are approximately twice as large in many areas. Again, the interpretation

295   of the observed trends is ambiguous, since there are individual members that resemble

296   observations (for example, member 1).

297

298   *b. Past trends (1972-2021) in the OBS LE*

299   The individual members of the OBS LE show a qualitatively similar diversity of 50-year

300   temperature trends as the CESM2 LE (Fig. 3). Like CESM2, some members show weak cooling

301   in some areas while others show widespread moderate or strong warming. This suggests that the

302   resemblance between the observed trend and the model's forced response may be purely

303   coincidental. Precipitation trends in the OBS LE also display large contrasts between members,

304   similar to CESM2 (Fig. 4). For example, nearly opposite patterns are found between members 6

305   and 11 (or 8 and 9). Trend amplitudes also vary considerably across the OBS LE, with larger

306   magnitudes in some members (for example, members 3 and 20) compared to others (e.g., members

307   21 and 13). While no single member of the 28 OBS LE samples shown matches the model's forced

308   trend, member 21 with its relatively muted trends comes close.

Observational large ensemble: Temperature trends 1972-2021

309
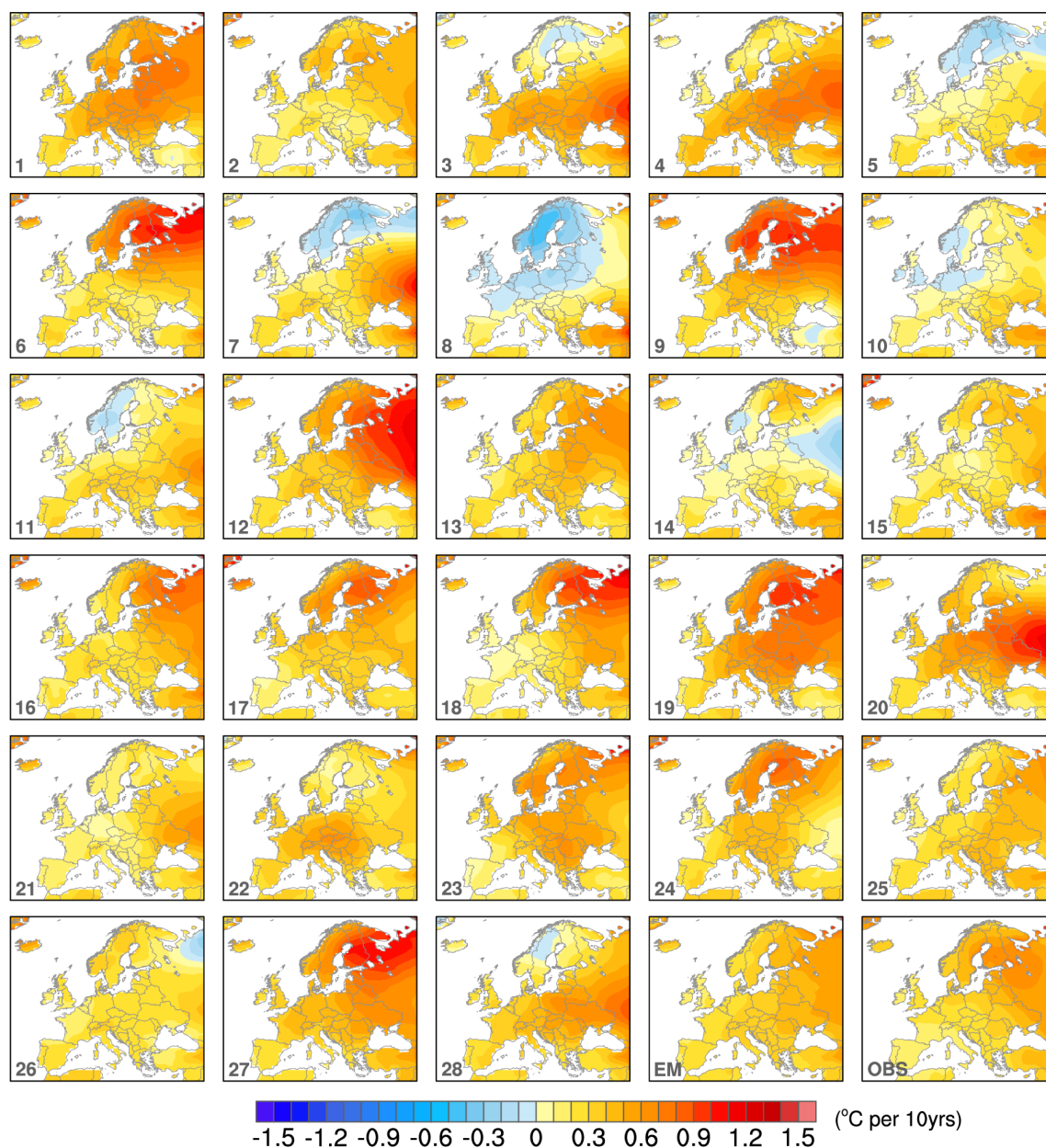
Figure 3. As in Fig. 1, but for the Observational Large Ensemble of McKinnon and Deser (2018)
with the ensemble-mean from the 100-member CESM2 Large Ensemble. See text for details.

312

Observational large ensemble: Precipitation trends 1972-2021

313
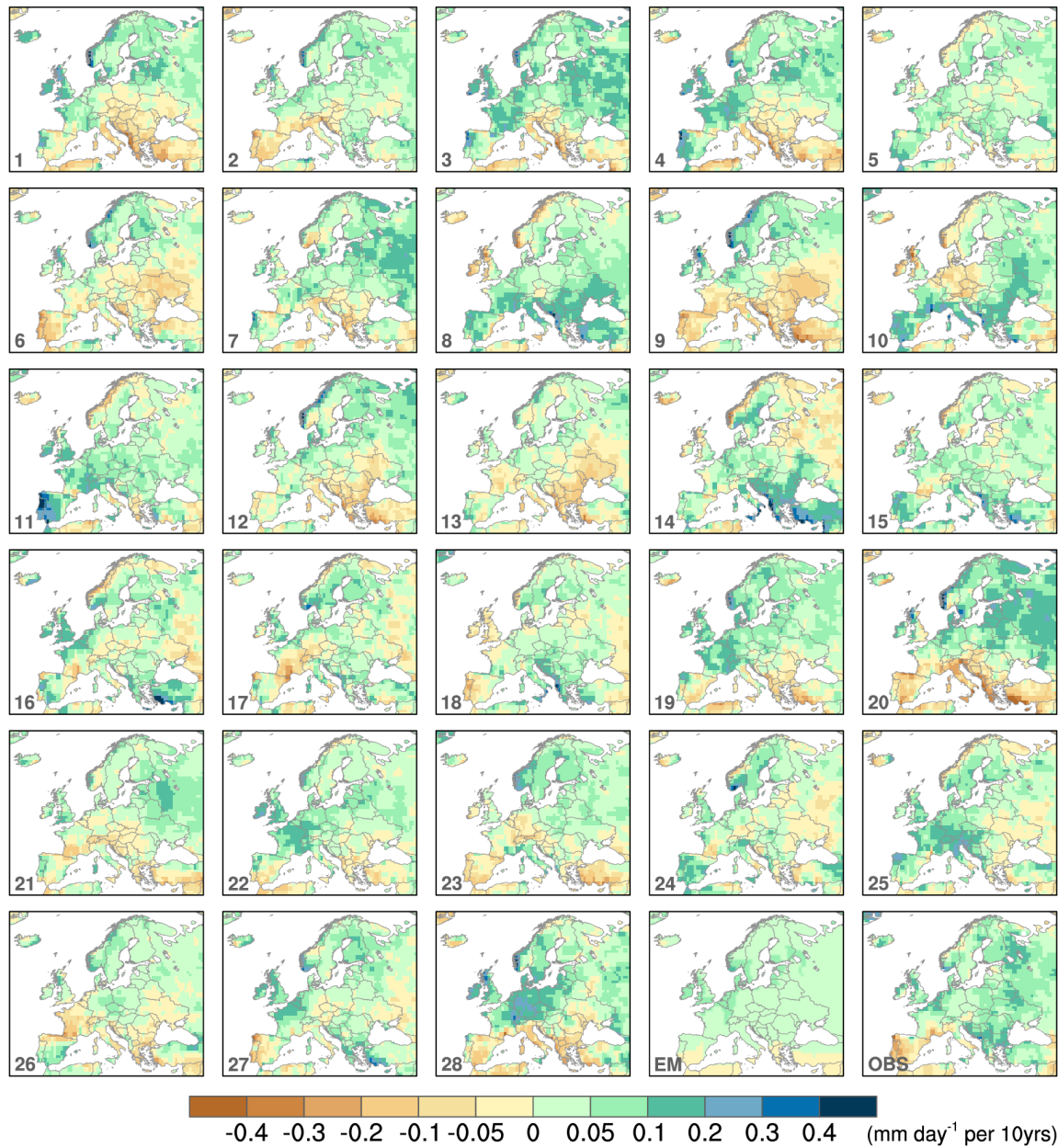
Figure 4. As in Fig. 2, but for the Observational Large Ensemble of McKinnon and Deser (2018) with the ensemble-mean from the 100-member CESM2 Large Ensemble. See text for details.

314
315
316

317   *c. Future Trends (2022-2071) in the CESM2 LE*

318   As expected, temperature trends projected for the next 50 years show larger amplitudes than those

319   for the past 50 years in the CESM2 LE (Fig. 5). This is due to the fact that the forced (ensemble-

320   mean) component of warming increases as greenhouse gas emissions accelerate. In most regions,

321   the forced warming trend increases by approximately 0.2°C per decade in the future compared to

322   the past. Notable exceptions are Iceland and the British Isles, which show less warming in the

323   future due to a circulation-induced forced cooling trend (see Section 3e). Despite a larger forced

324   component, temperature trends projected for the next 50 years still show a wide range of

325   amplitudes across individual members of the CESM2 LE. For example, member 13 is striking for

326   its muted warming (generally < 0.5°C per decade) across Europe (and absolute cooling over the

327   UK and Iceland), while member 28 shows highly amplified warming, with values exceeding 1.3

328   °C per decade over western Russia.

329

330   Forced trends in precipitation are projected to amplify over the next 50 years, with greater wetting

331   over northern Europe and drying over southern Europe and the Mediterranean (Fig. 6). In addition,

332   the region with a forced drying trend is projected to expand northward into Spain, Italy and the

333   Balkan Republics. While the forced pattern of future drying in the south and wetting in the north

334   is generally evident in most of the simulations shown, there are notable differences in amplitude

335   across the members. For example, member 28 shows precipitation trends in excess of 0.1 mm d^{-1}

336   per decade over most of northern Europe, while member 11 shows positive precipitation trends of

337   less than half this amount. Members 27 and 28 illustrate that the mid-section of the European

338   continent may get wetter or drier depending on the unpredictable sequence of internal variability

339   that unfolds. Thus, internal variability can still make a sizeable contribution to the projected

340   patterns and amplitudes of winter precipitation trends over the next 50 years.

341

342
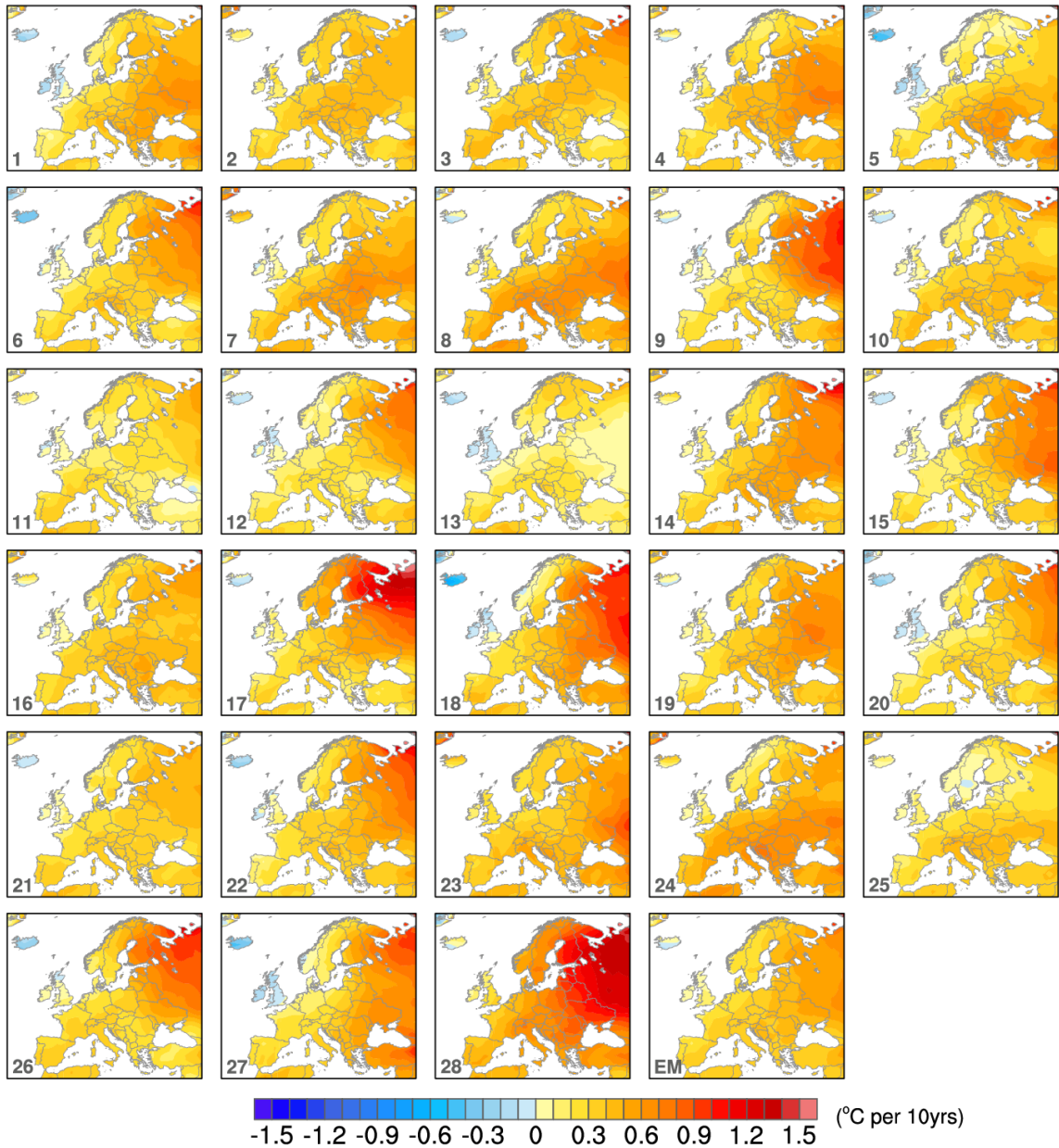
343   **Figure 5**. As in Fig. 1, but for the period 2022-2071.

344

345

CESM2 large ensemble: Precipitation trends 2022-2071
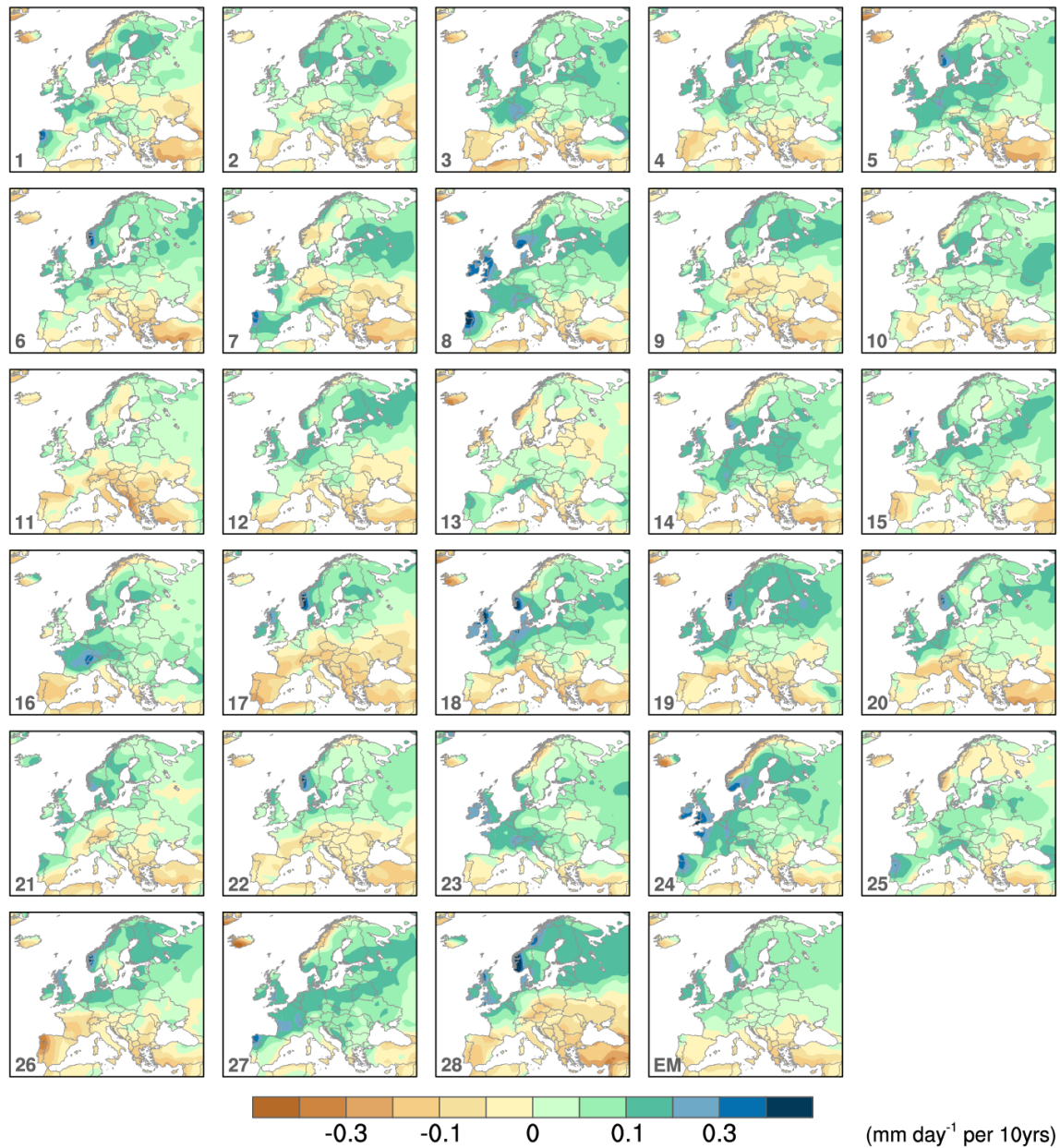
346
347
348 **Figure 6**. As in Fig. 2, but for the period 2022-2071.

349   *d. Signal-to-noise metrics and model evaluation.*

350   In the previous section, we conveyed a qualitative impression of the possible range of 50-year

351   trends due to the superposition of internal variability and forced climate change in the CESM2 and

352   OBS LEs. Here, we provide a more quantitative view, beginning with a comparison of the standard

353   deviation (σ) of trends over the period 1972-2021 computed across the ensemble members of each

354   LE. In the CESM2 LE, the ensemble σ of temperature trends increases from southwest to

355   northeast, with minimum values (0.05-0.10 K per decade) over Spain and northern Africa, and

356   maximum values (0.30-0.35 0.5°C per decade) over northwestern Russia (Fig. 7a). A similar

357   pattern is found in OBS LE, with some regional differences in amplitude (Fig. 7b). In particular,

358   the ensemble σ values are significantly smaller (20-40%) over Scandinavia, Germany and Poland,

359   and significantly larger (20-40%) in areas near the Mediterranean and Black Seas, in the OBS LE

360   compared to the CESM2 LE (Fig. 7c). For precipitation trends, the two LEs show similar patterns

361   of ensemble σ, with largest amplitudes generally along the west coasts (0.10 - 0.25 mm d^{-1} per

362   decade) and over southwestern Europe (values 0.05 – 0.10 mm d^{-1} per decade: Figs. 7d and e).

363   However, CESM2 LE significantly underestimates the OBS LE by more than 40% along the

364   Mediterranean and Black Seas and parts of Russia, and significantly overestimates the OBS LE by

365   20-40% in many areas of western Europe (Fig. 7f).
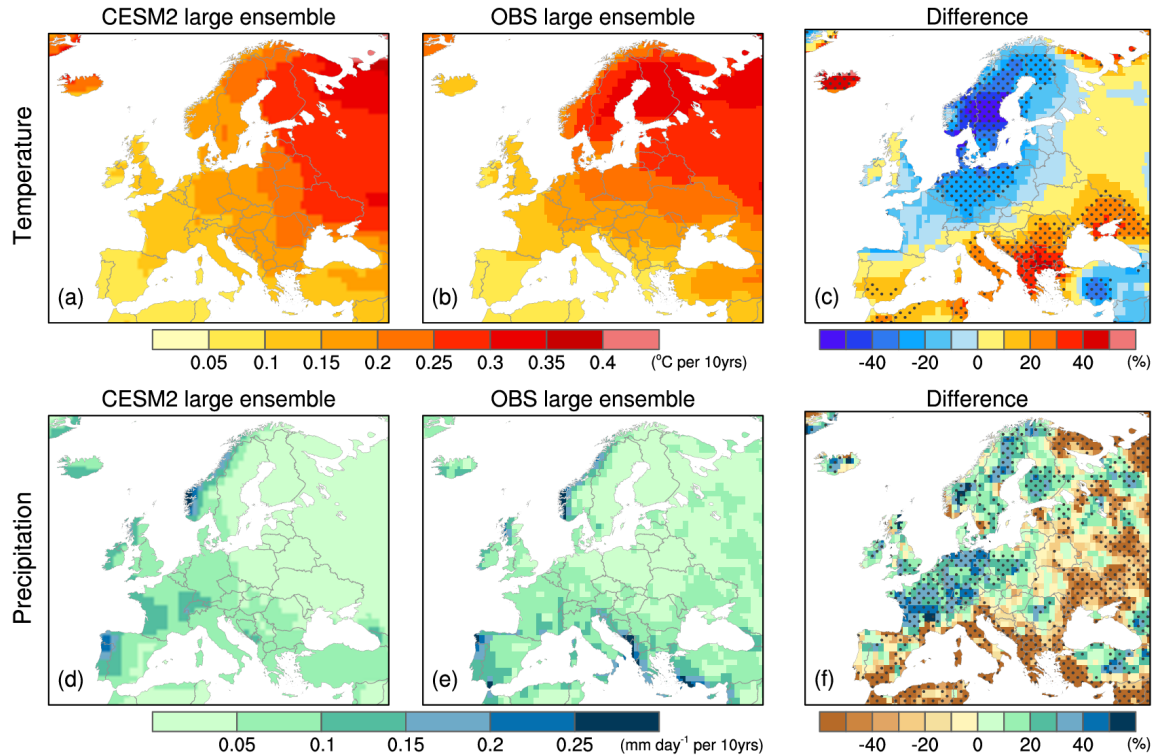
Figure 7. Standard deviation of 50-year trends (1972-2021) across 100 members of the CESM2 Large Ensemble (a,d) and 100 members of the Observational Large Ensemble (b,e), and their difference (c,f) for winter air temperature (top; °C per decade) and precipitation (bottom; mm d^{-1} per decade). Stippling in panels c and f indicates that the differences are statistically significant at the 95% confidence level according to an f-test.

Next, we assess the relative magnitude of the forced and internal components of trends by computing a "signal-to-noise" ratio defined as the CESM2 ensemble-mean trend divided by the σ of trends across the 100 members of each LE. This "signal-to-noise" ratio provides a metric of the likelihood that the ensemble-mean (e.g., forced) trend might be overwhelmed by the internally-generated trend in any given ensemble member (and by extension, the real world). Assuming that the 100-member set of 50-year trends follows a normal distribution (not shown, but see related results in Deser et al. 2012; Thompson et al. 2015; Deser et al. 2020a), a signal-to-noise ratio greater than one (two) indicates that the magnitude of the ensemble-mean (forced) trend is larger than (more than twice as large as) that of a typical (e.g., one standard deviation) internal trend, and

382 a signal-to-noise ratio less than one indicates that the amplitude of a typical internal trend exceeds

383 the magnitude of the forced trend. In the CESM2 LE, the signal-to-noise of forced temperature

384 trends over the past 50 years generally ranges from 1.5 - 2 over central and northern Europe, and

385 from 2-3 over southern Europe (Fig. 8a). Forced precipitation trends over the past 50 years exhibit

386 much lower signal-to-noise ratios than temperature, with values generally < 1 and nearly always

387 < 1.5 (Fig. 8d).

388

389
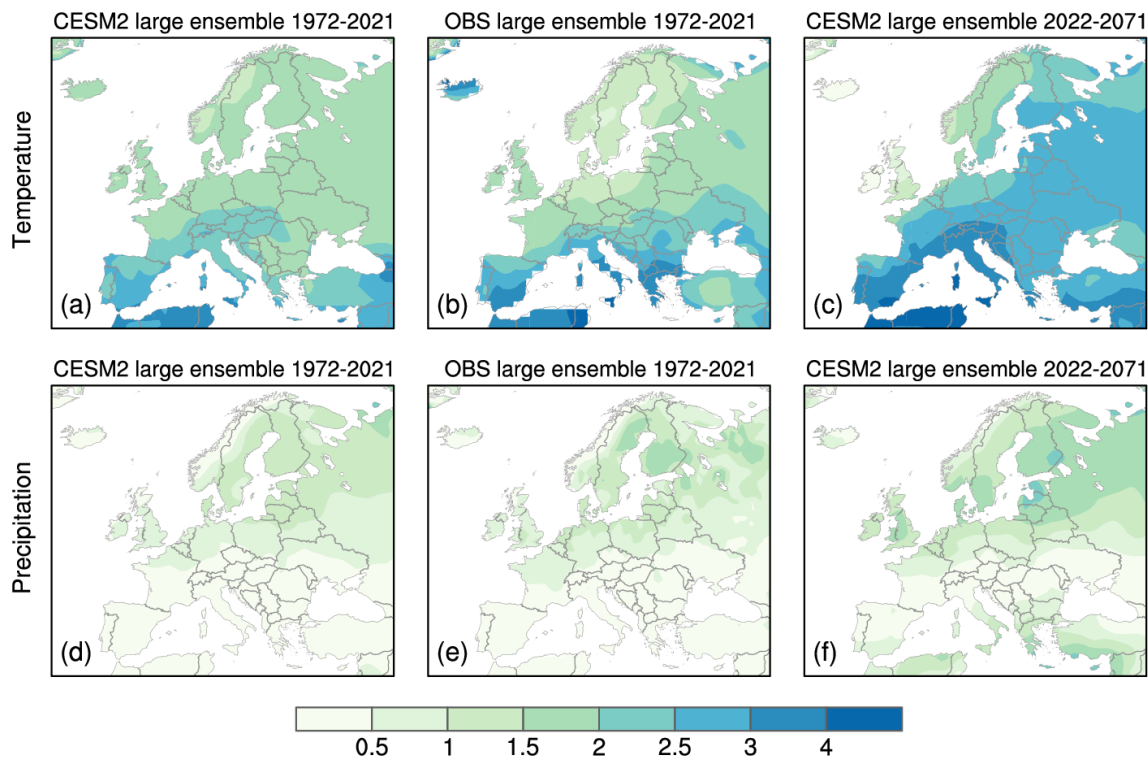
390 **Figure 8**.   Signal-to-noise of forced trends in winter (top) air temperature and (bottom)
391 precipitation based on the 100-member CESM2 Large Ensemble during 1972-2021 (a,d), the
392 Observational Large Ensemble during 1972-2021 (b,e), and the CESM2 Large Ensemble during
393 2022-2071 (c,f). See text for details.

394

395 How much do model biases in ensemble σ shown previously affect the signal-to-noise of the

396 model's forced trends? We address this question by using the OBS LE σ values in place of the

397   model's σ values in the signal-to-noise calculation (note that the "signal" in the two LEs is identical

398   by construction). This substitution results in an enhancement of signal-to-noise of past forced

399   temperature trends over southern Europe and a reduction in signal-to-noise over Scandinavia,

400   Germany and Poland, with a net increase from 38% to 60% in the area with values > 2 (Fig. 8b).

401   The impact of model biases in ensemble trend σ is much less pronounced for precipitation than

402   temperature, with signal-to-noise values in all locations remaining below 2 (Fig. 8e).

403

404   As expected, signal-to-noise values are higher for forced trends in the future than in the past.

405   Ninety-seven percent of the area of the continent (excluding Iceland and Greenland) shows a

406   signal-to-noise value > 2 for forced temperature trends during 2022-2071 (Fig. 8c), compared with

407   38% for trends during 1972-2021. Forced precipitation trends in the future remain uncertain, with

408   only 2% of the land area showing a signal-to-noise value > 2 (Fig. 8f).

409

410   Another way to view the relative impacts of internal variability and external forcing on trends is

411   by computing the fraction of ensemble members at each location that show a positive trend (e.g.,

412   warming or wetting). This metric conveys the likelihood of having a positive (or negative) trend

413   in any single ensemble member, which is analogous to the single "realization" of the real world.

414   At nearly all locations, more than 95% of ensemble members in the CESM2 LE show warming in

415   both the past and future periods, with slightly lower percentages (85-95%) over western

416   Scandinavia and parts of Great Britain (and < 75% over Ireland, Scotland and Iceland in the

417   future); (Figs. 9a and c). Similar percentages are obtained when the internal component of past

418   temperature trends in the OBS LE is used in place of the model's internal trends, with some

419   reduction (75-95%) over Scandinavia, northern Russia, Germany and Poland (Fig. 9b).

420
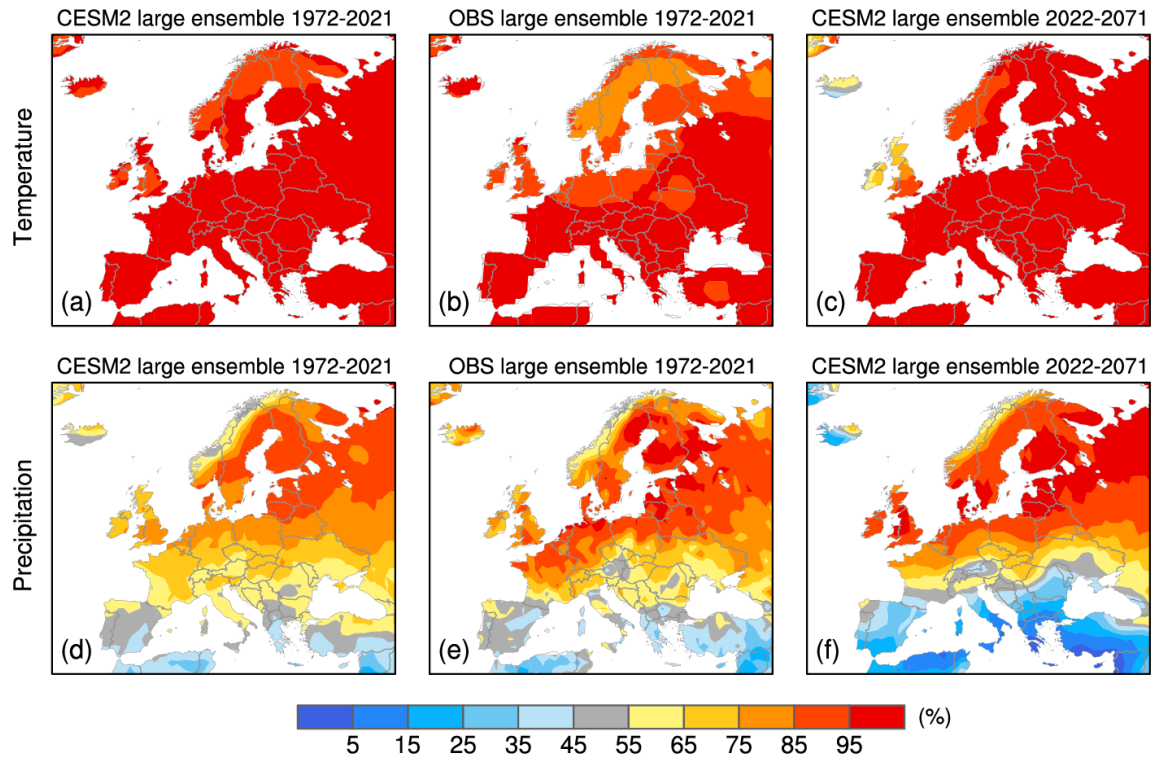
Figure 9. The percentage of ensemble members with a positive trend in winter (top) air temperature and (bottom) precipitation trends based on (a,d) the 100-member CESM2 Large Ensemble during 1972-2021, (b,e) the 100-member Observational Large Ensemble during 1972-2021, and (c,f) the 100-member CESM2 Large Ensemble during 2022-2071.

The sign of the trend in any given ensemble member is more uncertain for precipitation than for temperature. The highest chances (> 85%) of a positive precipitation trend are found over the northernmost third of the continent excluding Norway, both in the past and future (Figs. 9d and f). Similarly high chances of a negative precipitation trend (equivalent to < 15% of a positive trend) occur in areas near the Mediterranean Sea, but only in the future. The central portion of the continent shows roughly equal chances of having a positive or negative trend, both in the past and future. The area with a > 85% chance of a positive precipitation trend in the past 50 years expands southward into northern France, Germany and areas bordering the Baltic Sea when internal variability is derived from the OBS LE compared to the CESM2 LE (Fig. 9e).

436   Taken together, the results shown in Fig. 9 indicate that warming is virtually guaranteed at nearly

437   all locations, both in the past 50 years and the next 50 years, according to the CESM2 LE.

438   However, the sign of the precipitation trend (past and future) is robust only over the northern tier

439   of the continent, and only in the future over the Mediterranean region. The model results for past

440   trends are found to be generally credible as measured against the OBS LE, with some

441   overestimation in north-central Europe.

442

443   ***e. Range of outcomes and the role of the atmospheric circulation***

444   As the saying goes, "climate is what we expect, weather is what we get". This adage is also

445   applicable to climate change, where "human-induced climate change is what we expect, internal

446   variability plus human-induced climate change is what we get" (Deser 2020). Here, we illustrate

447   "what we expect" and the range of "what we get" for past and future 50-year trends in the CESM2

448   LE, using the ensemble-mean for "what we expect" and two contrasting ensemble members for

449   the range of "what we get". We select the contrasting members from the bottom and top 5th

450   percentiles of the distribution of 100-member trends averaged over the European continent for

451   each period separately. This selection criterion is somewhat arbitrary and does not necessarily

452   capture the wide range of trend amplitudes that may occur at a single location or sub-region, nor

453   does it portray the full range of spatial patterns that occur within the ensemble.

454

455   There is a large range in temperature trend outcomes ("what we get") for both the past 50 years

456   and the next 50 years as depicted by the "warm" and "cool" end-members (Fig. 10). For past

457   trends, the "warm" end-member shows temperature increases of 0.9-1.1 °C per decade over the

458   eastern portion of the continent (Fig. 10b), while the "cool" end-member displays muted warming

459
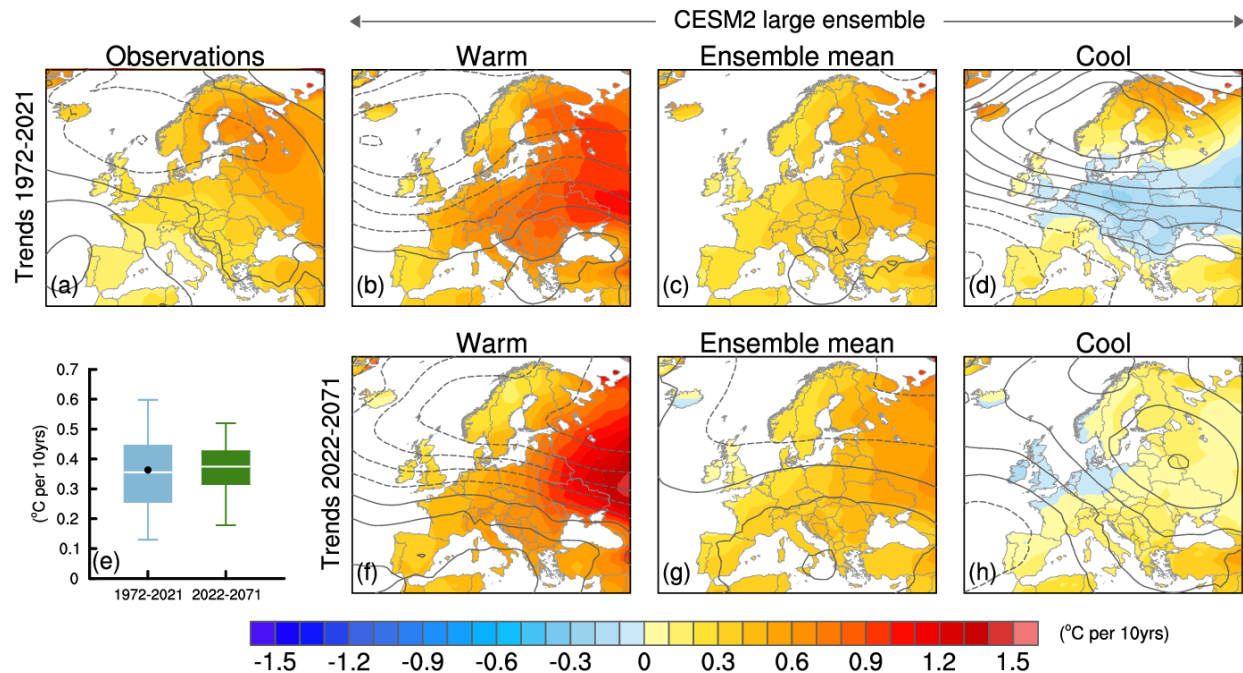
Figure 10. **A Range of Outcomes.** Trends in winter air temperature (color shading; °C per decade) and sea-level pressure (SLP) (contours; contour interval of 0.25 hPa per decade, negative values dashed) for the period (top) 1972-2021 and (bottom) 2022-2071. Panel (a) shows observed trends (1972-2021) and remaining panels show simulated trends from the 100-member CESM2 Large Ensemble: (c,g) ensemble-mean; (b,f) "warm" end-member; (d,h): "cool" end-member. See text for details. Note that panels (a) and (c) are identical to the "OBS" and "EM" panels in Fig. 1, respectively. Panel (e): Distribution of European-average trends for 1972-2021 (blue) and 2022-2071 (green) from the CESM2 Large Ensemble (box outlines 25th-to-75th percentile range, whiskers mark the 5th-to-95th percentile range, the horizontal white line denotes the median value, and the black circle marks the observed value).

(< 0.3 °C per decade) and even slight cooling through the midsection of the continent (Fig. 10d).

Clearly, the forced trend ("what we expect"), which depicts moderate warming (0.2-0.6°C per

decade) across the continent does not tell the whole story (Fig. 10c). Analogous results are found

for trends projected over the next 50 years: the "warm" member shows temperature increases of

1.0-1.5 °C per decade over west-central Russia (Fig. 10f) while the "cool" member depicts < 0.2°C

per decade warming over most of the continent (Fig. 10h), in marked contrast to the forced trend

which ranges from 0.3-0.6°C per decade (Fig. 10g). As discussed previously, the observed

temperature trend map resembles the model's ensemble-mean, but this could be by chance (Fig.

479   10a). In terms of European averages, the observed trend (0.36 °C per decade) is nearly coincident

480   with the median value of the model's trend distribution, which has a 5th-to-95th percentile range of

481   0.13-0.60 °C per decade for past 50-year trends (Fig. 10e). Curiously, the model's median trend

482   value for Europe as a whole increases only slightly in the future compared to the past, while the

483   5th-to-95th and 25th-to-75th percentile ranges narrow (Fig. 10e). Further work is needed to

484   understand why this is the case.

485

486   As mentioned in Section 1d, previous work has shown that internal variability of the large-scale

487   atmospheric circulation causes much of the member-to-member differences in temperature trends

488   in model LEs. Here, we provide a qualitative indication of the circulation influence by

489   superimposing SLP trends upon the maps in Fig. 10. In the case of past trends, the "warm" member

490   shows a positive North Atlantic Oscillation (NAO)-like pattern (Hurrell et al. 2003), with negative

491   SLP trends centered near Iceland and positive SLP trends centered over the Mediterranean (Fig.

492   10b). This SLP pattern is indicative of stronger westerly/southwesterly flow, which brings

493   relatively warm maritime air over the continent. The "cool" member shows a largely opposite

494   flow configuration (albeit with longitudinal shifts in the SLP centers-of-action), which advects

495   relatively cold air from the east over the continent (Fig. 10d). In comparison, the forced response

496   shows negligible atmospheric circulation change (Fig. 10c). Striking contrasts in circulation are

497   also found for the future period, with a large positive NAO-like trend pattern in the "warm"

498   member and a blocking continental "High" in the "cool" member (Figs. 10f and h). Future trends

499   in SLP also contain a modest forced component indicative of enhanced westerlies over the

500   continent (Fig. 10g).

501

502 The "wet" and "dry" end-members also show striking regional contrasts in both precipitation and

503 circulation (Fig. 11). For example, for past trends, the "wet" member shows precipitation increases

504 of 0.2-0.3 mm d^{-1} per decade over France, southern Germany, Portugal and the UK, and

505 precipitation declines over northern Norway and along the Mediterranean Sea (Fig. 11b). A nearly

506 opposite pattern is found for the "dry" member (Fig. 11d). These contrasting precipitation trends

507 can be understood in the context of the overlying atmospheric circulation changes, with wetter

508 areas coinciding with anomalous westerly/southwesterly flow and drier areas located under

509 blocking anticyclones. Analogous patterns are found for future trends, with pronounced increases

510 in precipitation over western Europe associated with the low pressure trend centered over the

511 British Isles in the "wet" member (Fig. 11f), and generally reduced precipitation in the "dry"

512 member associated with the blocking High centered over southern Europe (Fig. 11h).

513

514
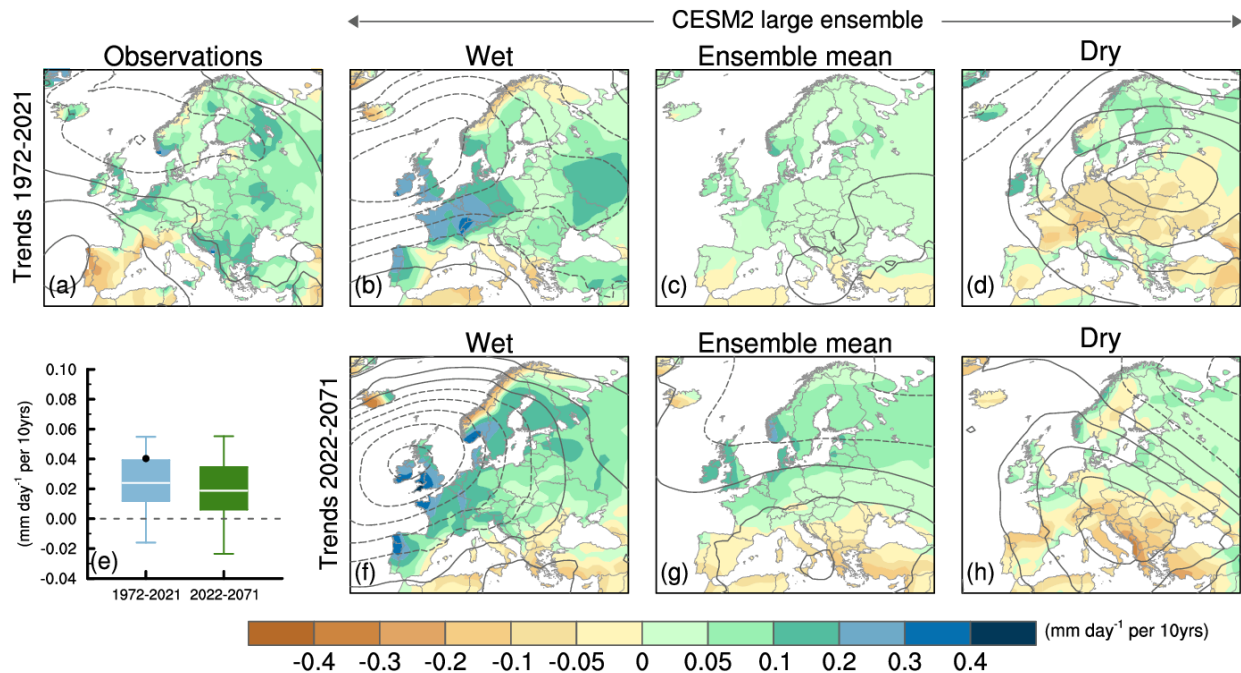
515 **Figure 11**. As in Fig. 10 but for precipitation (mm d^{-1} per decade). Note that panels (a) and (c)
516 are identical to the "OBS" and "EM" panels in Fig. 2, respectively.
517

518

f. Unmasking forced climate change in observations via "Dynamical Adjustment"

The empirical method of "dynamical adjustment" introduced in Section 1d can be used to estimate

the circulation-induced component of observed temperature anomalies; this dynamically-induced

contribution can then be subtracted from the original anomaly to obtain the thermodynamically-

induced component as a residual. Since this method uses no information from climate models, it

provides an independent estimate of the thermodynamic component of observed temperature

trends, which can be compared with the forced response simulated by climate model LEs.

526

Figure 12 shows the decomposition of observed DJF temperature trends into their dynamical and

residual thermodynamic contributions. For this example, we have used the 60-year period 1962-

2021 when observed SLP trends are more than twice as large as those during 1972-2021 on a per

decade basis (compare SLP contours in Figs. 10a and 12a). Observed SLP trends during the past

60 years show a pronounced positive NAO-like pattern, with maximum negative values of -1.25

hPa per decade near Iceland and maximum positive values of +0.75 hPa per decade west of Spain

(Fig. 12a). Enhanced westerly/southwesterly flow associated with this pattern advects warm air,

raising surface temperatures by 0.1- 0.3°C per decade (with maximum warming over northern

Europe) according to the dynamical adjustment algorithm (Fig. 12b). Removing this dynamically-

induced component from the total trend reveals the residual thermodynamic contribution to the

observed warming trend (Fig. 12c). This observed thermodynamic trend is much closer in

amplitude (and arguably pattern) to the model's forced response, given by the CESM2 LE

ensemble-mean trend (Fig. 12d), than is the total observed trend. Further, the lack of an

appreciable forced SLP trend in CESM2 indicates that the model's forced temperature trend is

541 thermodynamically-driven. The level of agreement between the observed thermodynamic

542 temperature trend and the model's forced thermodynamic trend leads to two powerful conclusions:

543 1) the model's forced temperature trend is realistic; and 2) removing the circulation-induced

544 component from the observed trends can effectively reveal the influence of anthropogenic forcing.

545 Analogous results have been found for North America (Deser et al. 2016).

546

547
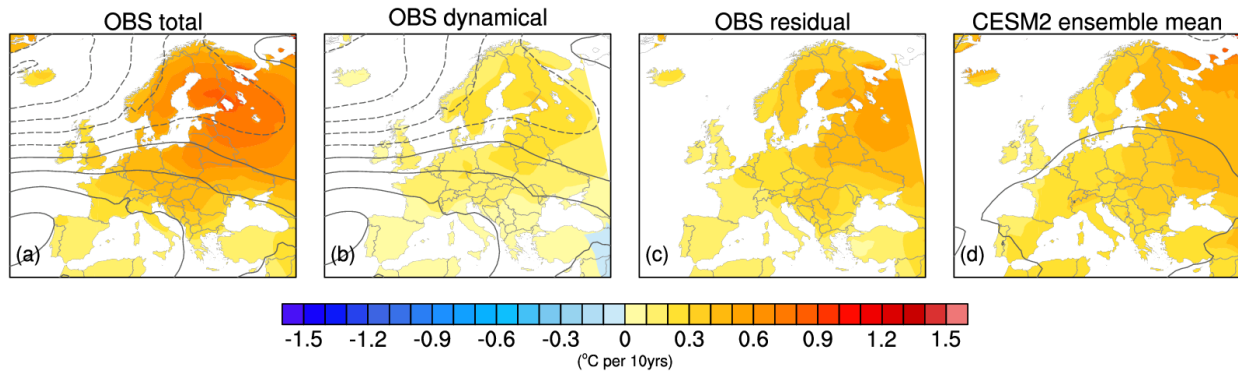
548 **Figure 12**. Decomposition of (a) observed winter air temperature trends (1962-2021; °C per
549 decade) into (b) dynamical and (c) residual thermodynamic contributions using the "dynamical
550 adjustment" procedure of Deser et al. (2018) based on constructed circulation analogues (see text
551 for details). Contours in (a) show observed sea-level pressure (SLP) trends (contour interval of
552 0.25 hPa per decade, negative values dashed); contours in (b) show the observed SLP trends
553 estimated from the constructed circulation analogues; contours in (c) based on the difference
554 between (a) and (b) are near-zero and not shown. Panel (d) shows the ensemble-mean temperature
555 and SLP trends from the 100-member CESM2 Large Ensemble (note that only the zero contour
556 shows up in panel d).

557

558 Precipitation is an inherently noisier field than temperature in both time and space, making it

559 challenging to extract the forced signal via "dynamical adjustment"; indeed, only one previous

560 study has attempted dynamical adjustment of observed precipitation trends (Guo et al. 2019).

561 Keeping in mind that the estimate of the circulation-induced component of precipitation trends

562 may be less robust than for temperature, we present the results as a proof-of-concept. Observed

563 precipitation trends during 1962-2021 are mainly driven by changes in atmospheric circulation,

564   with a small thermodynamic residual component (Fig. 13). This residual component bears some

565   resemblance to the forced response in CESM2, particularly in terms of amplitude (~ 0.05 mm d-1

566   per decade; Fig. 13d). Notable areas of agreement in the sign of the trends include drying over

567   much of southern Europe and wetting over parts of northern Europe; central Europe shows less

568   agreement in polarity, unsurprisingly since this region was found to have lower signal-to-noise

569   than other areas.

570

571
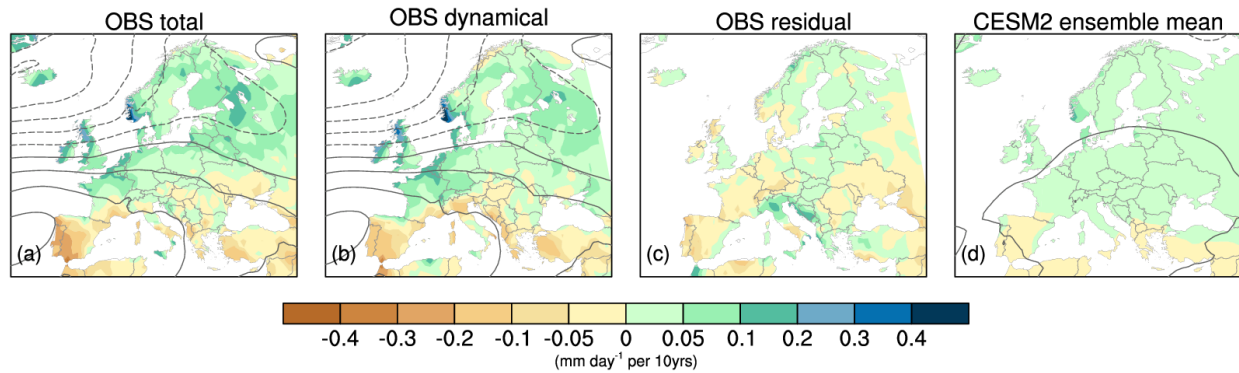
572   **Figure 13**. As in Fig. 12 but for precipitation (mm d^{-1} per decade).

573

574   *g. Toward an observationally-based "range of outcomes"*

575   We conclude by bringing together the results of the Observational LE and "dynamical adjustment"

576   to produce a fully observationally-based estimate of the range of past 60-year trends in temperature

577   and precipitation. To the best of our knowledge, this is first time that these two approaches have

578   been combined. Specifically, we add the internal component of trends from each member of the

579   OBS LE to the thermodynamic-residual trend (the estimated observed forced response) obtained

580   from dynamical adjustment. As before, we select two contrasting ensemble members from the tails

581   of the distribution based on European-wide averages to illustrate the range of trend outcomes. The

582   "warm" end-member shows pronounced temperature increases over the northern two-thirds of the

583   continent, with maximum values in excess of 0.9 °C per decade, while the "cool" end-member

584   warms less than 0.2 °C per decade in most areas and even cools slightly over Ukraine and

585   neighboring countries (Figs. 14 b and d, respectively). These divergent temperature trends are

586   associated with contrasting SLP trends, with a positive NAO-like pattern in the "warm" member

587   a negative (and eastward-shifted) NAO pattern in the "cool" member (Figs. 14 b and d).

588   Qualitatively, this range of trend outcomes for both temperature and SLP is remarkably similar to

589   that obtained directly from the CESM2 LE, with some regional differences in the location of

590   cooling in the "cool" end-member (Figs. 14 e and g). There is no guarantee that the patterns and

591   amplitudes of trends sampled in our selected end-members will agree between the model and

592   observationally-based results, since there are many configurations that produce extremes in

593   European-wide averages (not shown). That there is a strong qualitative resemblance between them

594   is a testament to both the realism of the model's forced response and internal variability, and the

595   efficacy of the OBS LE and dynamical adjustment approaches.

596

597
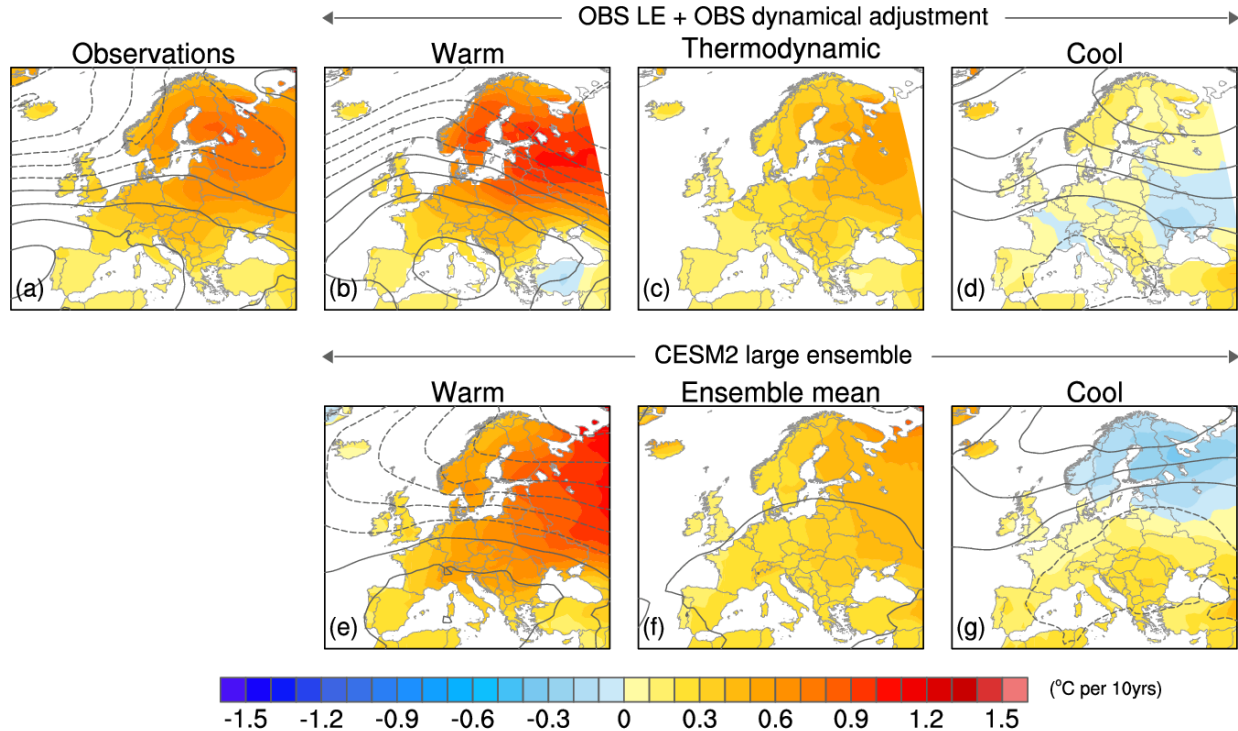
Figure 14. As in Fig. 10 but for the period 1962-2021. The top row is based on the Observational Large Ensemble combined with the residual thermodynamic component of observed trends. The bottom row is based on the 100-member CESM2 Large Ensemble. See text for details.

Precipitation trends in the "wet" and "dry" end-members are also similar between the model and observationally-based results (Fig. 15). The "wet" members show widespread increases in precipitation over southern and central Europe (maximum values of 0.2-0.4 mm d^{-1} per decade) and drying over the northern UK and parts of Scandinavia (Figs. 15 b and e). Largely opposite patterns prevail in the "dry" members (Figs. 15 d and g). The contrasting precipitation trends in the "wet" and "dry" end-members are associated with opposite flow configurations, with regions of drying corresponding to high pressure and vice versa.
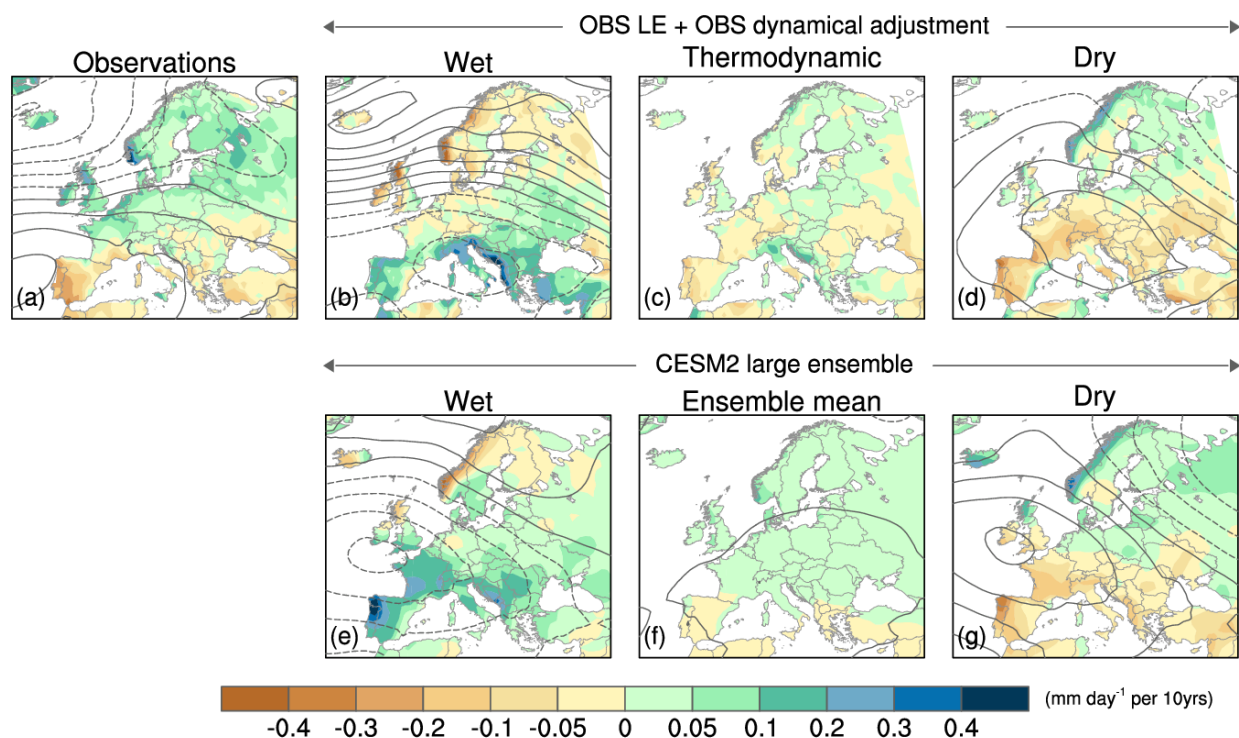
Figure 15. As in Fig. 14 but for precipitation (mm d^{-1} per decade).

4. Summary and open questions

Disentangling the effects of internal variability and anthropogenic forcing on regional climate trends remains a long-standing issue in climate sciences. Recent advances in climate modeling and physical understanding have led to new insights on this topic and provided an improved source of information on the future risks of weather extremes associated with human-induced climate change. Here, we have highlighted new findings for European winter climate based on the following complementary tools: Earth System Model Large Ensemble simulations; an observationally-based Large Ensemble; and an empirical approach for removing the influence of atmospheric circulation variability from observed temperature and precipitation data, termed "dynamical adjustment".

623   The new 100-member CESM2 Large Ensemble shows that internal climate variability imparts

624   considerably uncertainty to past and future 50-year trends in winter temperature and precipitation

625   over Europe. Such uncertainty is irreducible due to the lack of predictability of the simulated

626   internal variability on decadal time scales. A novel synthetic Large Ensemble constructed from the

627   statistical characteristics of internal variability in the observational record exhibits quantitatively

628   similar levels of uncertainty in past 50-year trends as the CESM2 LE, reinforcing the credibility

629   of the model's internally-generated trends. Additionally, the results of our "dynamical adjustment"

630   procedure applied to observations shows good agreement between the observed thermodynamic-

631   residual trend component and the model's forced thermodynamic trend, further underscoring the

632   realism of CESM2. Finally, we have combined internal variability of trends from an Observational

633   Large Ensemble with an observational estimate of the forced trend (the thermodynamic-residual

634   component obtained from "dynamical adjustment") to show what the observed range of past trends

635   in European temperature and precipitation could have been. Because it does not rely on climate

636   model information, this observationally-based range of trend outcomes provides a powerful test of

637   the range of simulated trends in a model Large Ensemble. To the best of our knowledge, this is the

638   first time that such a synthesis of the two purely observational methods has been undertaken.

639

640   Many outstanding questions remain regarding the relative influences of internal climate variability

641   and anthropogenic forcing on regional climate change in models and the real world. Fortunately,

642   promising new tools are being developed to help address these challenges. For example, innovative

643   machine learning methods may be able to improve upon existing techniques for constructing

644   Observational Large Ensembles. Such methods have shown good results as statistical emulators

645   of model-based LEs, but their application to the observational record remains to be pursued

646   (Beusch et al. 2019). Similarly, neural network approaches to dynamical adjustment may offer

647   increased skill compared to conventional methods (Davenport and Diffenbaugh, 2021), but have

648   yet to be applied with the aim of separating forced and internal components of observed trends.

649   Complementary physically-based approaches such as Linear Inverse Modeling and Low-

650   Frequency Pattern Analysis mentioned in Section 1d also offer promise for estimating the forced

651   response in observations without reliance on climate models and should be pursued more widely.

652

653   We have relied on the fact that the CESM2 LE (like other models of its class; see Deser et al.

654   2020a and references therein) simulates a negligible forced atmospheric circulation trend over the

655   past 50-60 years to interpret our observed dynamical adjustment results (i.e, we have equated the

656   observed dynamically-induced trend with the internal component, and the observed

657   thermodynamic-residual trend with the forced component). If the model is erroneous in this regard,

658   then our interpretation of our decomposition of observed trends into "internal dynamical" and

659   "forced thermodynamic" components is flawed. Indeed, recent work suggests that climate models

660   may be less predictable on seasonal-to-decadal timescales than the real world, particularly in terms

661   of the large-scale extra-tropical atmospheric circulation (the so-called "signal-to-noise" paradox,

662   e.g., Scaife et al. 2014; Eade et al. 2014; Scaife and Smith, 2018). But whether the results from

663   such initial-value predictability studies carry over to models' forced atmospheric circulation

664   responses to anthropogenic emissions remains an open question. Finally, a recent study by

665   Strommen et al. (2002) finds that inclusion of stochastic parameterizations amplifies the simulated

666   atmospheric circulation response to sea surface temperature and Arctic sea ice anomalies. Such

667   stochastic parameterizations may represent unresolved air-sea coupling processes in "coarse-

668   resolution" climate models such as CESM2. Emerging efforts to develop mesoscale-eddy-

669   resolving global coupled climate models may provide more definitive answers to this elusive

670   challenge in the near future.

671

672   **Data and code availability statement**

673   All data used in this study are publicly available as follows:

674   CESM2 Large Ensemble: https://www.earthsystemgrid.org/dataset/ucar.cgd.cesm2le.output.html

675   GPCC precipitation: https://www.dwd.de/EN/ourservices/gpcc/gpcc.html

676   BEST temperature: http://berkeleyearth.org/data/

677   and ERA5 SLP: https://www.ecmwf.int/en/forecasts/dataset/ecmwf-reanalysis-v5

678   Code used to create the Observational Large Ensemble and Dynamical Adjustment results are

679   publicly available at:

680   https://github.com/karenamckinnon/observational_large_ensemble/ and

681   https://github.com/terrayl/Dynamico, respectively.

682

683   **Author contributions**

684   CD led the overall effort and wrote the manuscript. ASP performed some of the calculations and

685   prepared the figures.

686

687   **Competing interests**

688   The contact author has declared that none of the authors has any competing interests.

689

690   **Acknowledgements**

691   We acknowledge the efforts of all those who contributed to producing the model simulations and

692   observational data sets used in this study. We thank the Reviewers for their constructive comments

693   and suggestions, Dr. Laurent Terray for providing the dynamical adjustment results and Dr. Karen

694   McKinnon for providing the observational large ensemble results. The National Center for

695   Atmospheric Research is sponsored by the National Science Foundation.

696

References

Andrews, T., Bodas-Salcedo, A., Gregory, J. M., Dong, Y., Armour, K. C., Paynter, D., Lin, P., Modak, A., Mauritsen, T., Cole, J. N. S., Medeiros, B., Benedict, J. J., Douville, H., Roehrig, R., Koshiro, T., Kawai, H., Ogura, T., Dufresne, J. -L., Allan, R. P., and Liu, C.: On the effect of historical SST patterns on radiative feedback, J. Geophys. Res.-Atmos., 127, e2022JD036675, https://doi.org/10.1029/2022JD036675, 2022.

Barnes, E. A., Hurrell, J. W., and Uphoff, I. E.: Viewing forced climate patterns through an AI lens, Geophys. Res. Lett., 46, 13389–13398, https://doi.org/10.1029/2019GL084944, 2019.

Beusch, L., Gudmundsson, L., and Seneviratne, S. I.: Emulating Earth System Model temperatures: from global mean temperature trajectories to grid-point level realizations on land, Earth Syst. Dyn. Discuss., https://doi.org/10.5194/esd-2019-34, 2019.

Bódai, T., G. Drótos, M. Herein, F. Lunkeit, and V. Lucarini: The Forced Response of the El Niño–Southern Oscillation–Indian Monsoon Teleconnection in Ensembles of Earth System Models. *J. Climate*, 33, 2163–2182, https://doi.org/10.1175/JCLI-D-19-0341.1, 2020.

Bódai, T., J.-Y. Lee, and A. Sundaresan: Sources of Nonergodicity for Teleconnections as Cross-Correlations, *Geophys. Res. Lett.*, 49, 8, e2021GL096587, doi: 10.1029/2021GL096587, 2022.

Bonfils, C. J. W., Santer, B. D., Fyfe, J. C., Marvel, K., Phillips, T. J., and Zimmerman, S. R. H.: Human influence on joint changes in temperature, rainfall and continental aridity. Nat. Clim. Change, 10, 726-731, https://doi.org/10.1038/s41558-020-0821-1, 2020.

Branstator, G. and Teng, H.: Two limits of initial-value decadal predictability in a CGCM, J. Climate, 23, 6292-6311, https://doi.org/10.1175/2010JCLI3678.1, 2010.

720   Capotondi, A., Deser, C., Phillips, A., Okumura, Y. and Larson, S.: ENSO and Pacific

721   DecadalVvariability in the Community Earth System Model Version 2, J. Adv. Model.

722   Earth Sy., 12, e2019MS002022, https://doi.org/10.1029/2019MS002022, 2020.

723   Compo, G. P., Whitaker, J. S., Sardeshmukh, P. D., Matsui, N., Allan, R. J., Yin, X., Gleason,

724   B.E., Vose, R.S., Rutledge, G., Bessemoulin, P., Brönnimann, S., Brunet, M., Crouthamel,

725   R.I., Grant, A.N., Groisman, P.Y., Jones, P.D., Kruk, M.C., Kruger, A.C., Marshall, G.J.,

726   Maugeri, M., Mok, H.Y., Nordli, Ø., Ross, T.F., Trigo, R.M., Wang, X.L., Woodruff, S.D.

727   and Worley, S.J.: The twentieth century reanalysis project, Q. J. Roy. Meteor. Soc., 137, 1–

728   28, https://doi.org/10.1002/qj.776, 2011.

729   Davenport, F. V. and Diffenbaugh, N. S.: Using machine learning to analyze physical causes of

730   climate change: A case study of U.S. Midwest extreme precipitation, Geophys. Res.

731   Lett., 48, e2021GL093787. https://doi.org/10.1029/2021GL093787, 2021.

732   Deser, C., Phillips, A., Bourdette, V., and Teng, H. Y.: Uncertainty in climate change

733   projections: The role of internal variability, Clim. Dynam., 38, 527–546.

734   https://doi.org/10.1007/s00382-010-0977-x, 2012.

735   Deser, C., Phillips, A., Alexander, M. A., and Smoliak, B. V.: Projecting North American

736   climate over the next 50 years: Uncertainty due to internal variability. J. Climate, 27, 2271–

737   2296, https://doi.org/10.1175/JCLI-D-13-00451.1, 2014.

738   Deser, C., Terray, L., and Phillips, A. S.: Forced and internal components of winter air

739   temperature trends over North America during the past 50 years: Mechanisms and

740   implications, J. Climate, 29, 2237–2258. https://doi.org/10.1175/JCLI-D-15-0304.1, 2016.

741   Deser, C., Simpson, I. R., McKinnon K. A., and Phillips, A. S.: The Northern Hemisphere extra-

742   tropical atmospheric circulation response to ENSO: How well do we know it and how do

743   we evaluate models accordingly? J. Climate, 30, 5059-5082, https://doi.org/10.1175/JCLI-

744   D-16-0844.1, 2017.

745 Deser, C., Hurrell, J. W., and Phillips, A.S.: The role of the North Atlantic Oscillation in

746   European Climate Projections, Clim. Dynam., 49, 3141–3157,

747   https://doi.org/10.1007/s00382-016-3502-z, 2017.

748 Deser, C., Simpson, I. R., Phillips, A. S., and McKinnon, K.A.: How well do we know ENSO's

749   climate impacts over North America, and how do we evaluate models accordingly? J.

750   Climate, 30, 4991-5014, https://doi.org/10.1175/JCLI-D-17-0783.1, 2018.

751 Deser, C.: Certain uncertainty: The role of internal climate variability in projections of regional

752   climate change and risk management. Earths Future, 8, e2020EF001854,

753   https://doi.org/10.1029/2020EF001854, 2020.

754 Deser, C., Lehner, F., Rodgers, K. B., Ault, T., Delworth, T. L., DiNezio, P. N., Fiore, A.,

755   Frankignoul, C., Fyfe, J. C., Horton, D. E., Kay, J. E., Knutti, R., Lovenduski, N. S.,

756   Marotzke, J., McKinnon, K. A., Minobe, S., Randerson, J., Screen, J. A, Simpson, I. R.,

757   and Ting, M.: Insights from earth system model initial-condition large ensembles and

758   future prospects. Nat. Clim. Change, 10, 277-286, https://doi.org/10.1038/s41558-020-

759   0731-2, 2020a.

760 Deser, C., Phillips, A. S., Simpson, I. R., Rosenbloom, N., Coleman, D., Lehner, F., Pendergrass,

761   A., DiNezio, P., and Stevenson, S.: Isolating the Evolving Contributions of Anthropogenic

762   Aerosols and Greenhouse Gases: A New CESM1 Large Ensemble Community Resource. J.

763   Climate, 33, 7835-7858, https://doi.org/10.1175/JCLI-D-20-0123.1, 2020b.

764 Deser, C. and Phillips, A.S.: Defining the internal component of Atlantic Multidecadal

765   Variability in a changing climate. Geophys. Res. Lett., 48, e2021GL095023,

766   https://doi.org/10.1029/2021GL095023, 2021.

767 DiNezio, P. N., Deser, C., Okumura, Y., and Karspeck, A.: Predictability of 2-year La Niña

768   events in a coupled general circulation model, Clim. Dyn. 49, 4237–4261, 2017.

769 Dong, Y, Armour, K.C., Zelinka, M., Proistosescu, C., Battisti, D., Zhou, C., and Andrews, T.:

770   Inter-model spread in the pattern effect and its contribution to climate sensitivity in CMIP5

771   and CMIP6 models, J. Climate, https://doi.org/10.1175/JCLI-D-19-1011.1, 2020.

772 Eade, R., Smith, D., Scaife, A., Wallace, E., Dunstone, N., Hermanson, L., and Robinson, N.: Do

773   seasonal-to-decadal climate predictions underestimate the predictability of the real

774   world?, Geophys. Res. Lett., 41, 5620– 5628, https://doi.org/10.1002/2014GL061146,

775   2014.

776 Fasullo, J. T. and R.S. Nerem: "Altimeter-era emergence of the patterns of forced sea-level rise

777   in climate models and implications for the future. *Proc. Natl Acad. Sci.*

778   https://doi.org/10.1073/pnas.1813233115, 2018.

779 Fasullo, J., Phillips, A. S., and Deser, C.: Evaluation of leading modes of climate variability in

780   the CMIP Archives, J. Climate, 33, 5527–5545, https://doi.org/10.1175/JCLI-D-19-1024.1,

781   2020.

782 Gordon, E. M. and Barnes, E.A.: Incorporating uncertainty into a regression neural network

783   enables identification of decadal state-dependent predictability, Geophys. Res. Lett.,

784   e2022GL098635, https://doi.org/10.1029/2022GL098635, 2022.

785 Gould, S. J.: Wonderful Life: The burgess shale and the nature of history, W. W. Norton & Co.,

786   978-0-393-30700-9, 1989.

787 Griffies, S. M. and Bryan, K.: Predictability of North Atlantic multidecadal climate

788   variability, Science, 275, 181–184, https://doi.org/10.1126/science.275.5297.181, 1997.

789 Guo, R. X., Deser, C., Terray, L., and Lehner, F.: Human influence on terrestrial precipitation

790   trends revealed by dynamical adjustment, Geophys. Res. Lett., 46, 3426-3434,

791   https://doi.org/10.1029/2018GL081316, 2019.

792 Hegerl, G.C., Zwiers, F. W. , Braconnot, P., Gillett, N. P., Luo, Y., Marengo Orsini, J. A.,

793   Nicholls, N., Penner, J. E., and Stott, P. A.: Understanding and attributing climate change.

794   In: Climate Change 2007: The Physical Science Basis. Contribution of Working Group I to

795   the Fourth Assessment Report of the Intergovernmental Panel on Climate Change,

796   Solomon, S., D. Qin, M. Manning, Z. Chen, M. Marquis, K.B. Averyt, M. Tignor and H.L.

797   Miller (eds.), Cambridge University Press, Cambridge, United Kingdom and New York,

798   NY, USA, 2007.

799 Hurrell J. W., Kushnir, Y., Ottersen G., and Visbeck M. (eds): The North Atlantic Oscillation:

800   climate significance and environmental impact, Geophys. Monogr. Ser, 134, AGU,

801   Washington, D. C, 2003.

802 James, I. N. and James, P. M.: Spatial structure of ultra-low-frequency variability of the flow in a

803   simple atmospheric circulation model. Quart. J. Roy. Meteor. Soc., 118, 1211-1233,

804   https://doi.org/10.1002/qj.49711850810, 1992.

805 Jin, E.K., Kinter, J.L., and Wang, B: Current status of ENSO prediction skill in coupled ocean–

806   atmosphere models, Clim. Dynam. 31, 647–664, https://doi.org/10.1007/s00382-008-0397-

807   3, 2008.

808 Kay, J., Deser, C., Phillips, A., Mai, A., Hannay, C., Strand, G., Arblaster, J. M., Bates, S. C.,

809   Danabasoglu, G., Edwards, J., Holland, M., Kushner, P., Lamarque, J. -F., Lawrence, D.,

810   Lindsay, K., Middleton, A., Munoz, E., Neale, R., Oleson, K., Polvani, L. and Vertenstein,

811   M.: The Community Earth System Model (CESM) Large Ensemble Project: A community

812   resource for studying climate change in the presence of internal climate variability, B. Am.

813   Meteorol. Soc., 96, 1333–1349, https://doi.org/10.1175/BAMS-D-13-00255.1, 2015.

814   Klavans, J.M., Cane, M.A., Clement, A.C., and Murphy, L. N.: NAO predictability from external

815   forcing in the late 20th century, Npj Clim. Atmos. Sci., 4, 22 (2021),

816   https://doi.org/10.1038/s41612-021-00177-8, 2021.

817   Lehner, F., Schurer, A. P., Hegerl, G. C., Deser, C., and Frölicher, T. L.: The importance of

818   ENSO phase during volcanic eruptions for detection and attribution, Geophys. Res. Lett.

819   43, 2851–2858, https://doi.org/10.1002/2016GL067935, 2016.

820   Lehner, F., Deser, C., and Terray, L.: Towards a new estimate of "time of emergence" of

821   anthropogenic warming: insights from dynamical adjustment and a large initial-condition

822   model ensemble. J. Climate, 30, 7739-7756, http://doi.org/10.1175/JCLI-D-16-0792.1,

823   2017.

824   Lehner, F., Deser, C., Simpson, I. R., and Terray, L.: Attributing the US Southwest's recent shift

825   into drier conditions, Geophys. Res. Lett., 45, 6251–6261,

826   https://doi.org/10.1029/2018GL078312, 2018.

827   Lehner, F., Deser, C., Maher, N., Marotzke, J., Fischer, E., Brunner, L., Knutti, R. and Hawkins,

828   E.: Partitioning climate projection uncertainty with multiple large ensembles and

829   CMIP5/6. Earth Syst. Dynam. Discuss., Special Issue on Large Ensembles, 11, 491–508,

830   https://doi.org/10.5194/esd-11-491-2020, 2020.

831   Leith, C. E.: The standard error of time-average estimates of climatic means, J. Appl. Meteorol.

832   Clim., 12(6), 1066-1069, https://doi.org/10.1175/1520-

833   0450(1973)012%3C1066:TSEOTA%3E2.0.CO;2, 1973.

834   Lorenz, E. N.: Deterministic nonperiodic flow, J. Atmos. Sci., 20, 130–141,

835   https://doi.org/10.1175/1520-0469(1963)020<0130:DNF>2.0.CO;2, 1963.

836   Madden, R. A.: Estimates of the natural variability of time-averaged sea-level pressure, Mon.

837   Weather. Rev., 104, 942-952, https://doi.org/10.1175/1520-

838   0493(1976)104%3C0942:EOTNVO%3E2.0.CO;2, 1975.

839   Maher, N., Matei, D., Milinski, S., and Marotzke, J.: ENSO change in climate projections:

840   Forced response or internal variability?, Geophys. Res. Lett., 45, 11390–11398,

841   https://doi.org/10.1029/2018GL079764, 2018.

842   Maher, N., Milinski, S., Suarez-Gutierrez, L., Botzet, M., Dobrynin, M., Kornblueh, L., Kröger,

843   J., Takano, Y., Ghosh, R., Hedemann, C., Li, C., Li, H., Manzini, E., Notz, D. Putrasahan,

844   D., Boysen, L., Claussen, M., Ilyina, T., Olonscheck, D., Raddatz, T., Stevens, B., and

845   Marotzke, J.: The Max Planck Institute Grand Ensemble: Enabling the exploration of

846   climate system variability, J. Adv. Model. Earth Sy., 11, 2050–2069,

847   https://doi.org/10.1029/2019MS001639, 2019.

848   McGraw, M. C., Barnes, E. A., and Deser, C.: Reconciling the observed and modeled southern

849   hemisphere circulation response to volcanic eruptions, Geophys. Res. Lett., 43, 7259–7266,

850   https://doi.org/10.1002/2016GL069835, 2016.

851   McKenna, C. M., and Maycock, A. C.: Sources of uncertainty in multimodel large ensemble

852   projections of the winter North Atlantic Oscillation, Geophys. Res. Lett., 48,

853   e2021GL093258, https://doi.org/10.1029/2021GL093258, 2021.

McKinnon, K. A and Deser, C.: Internal variability and regional climate trends in an
Observational Large Ensemble, J. Climate, 31, 6783–6802, https://doi.org/10.1175/JCLI-D-17-0901.1, 2018.

McKinnon, K. A. and Deser, C.: The inherent uncertainty of precipitation variability, trends, and
extremes due to internal variability, with implications for Western US water resources, J.
Climate, 34, 9605-9622, https://doi.org/10.1175/JCLI-D-21-0251.1, 2021.

Meehl, G., Hu, A. and Teng, H: Initialized decadal prediction for transition to positive phase of
the Interdecadal Pacific Oscillation, Nat. Commun., 7, 11718 (2016),
https://doi.org/10.1038/ncomms11718, 2016.

Meehl, G.A., J.H. Richter, Teng, H., Capotondi, A., Cobb, K., Doblas-Reyes, F., Donat, M. G.,
England, M. H., Fyfe, J. C., Han, W., Kim, H., Kirtman, B. P., Kushnir, Y., Lovenduski, N.
S., Mann, M. E., Merryfield, W. J., Nieves, V., Pegion, K., Rosenbloom, N., Sanchez, S.
C., Scaife, A. A., Smith, D., Subramanian, A. C., Sun, L., Thompson, D., Ummenhofer, C.
C., and Xie, S. -P.: Initialized Earth system prediction from subseasonal to decadal
timescales, Nat. Rev. Earth Environ., 2, 340–357 (2021), https://doi.org/10.1038/s43017-021-00155-x, 2021.

Merrifield, A., Lehner, F., Xie, S. -P., and Deser, C.: Removing circulation effects to assess
Central US land-atmosphere interactions in the CESM Large Ensemble, Geophys. Res.
Lett., 44, 9938-9946, https://doi.org/10.1002/2017GL074831, 2017.

Milinski, S., Maher, N., and Olonscheck, D.: How large does a large ensemble need to be?, Earth
Syst. Dyn. Discuss., 11, 885-901, https://doi.org/10.5194/esd-11-885-2020, 2019.

Newman, M.: Interannual to decadal predictability of tropical and North Pacific sea surface
temperatures, J. Climate, 20, 2333–2356, https://doi.org/10.1175/JCLI4165.1, 2007.

877   Newman, M., Alexander, M. A., Ault, T. R., Cobb, K. M., Deser, C., Di Lorenzo, E., Mantua, N.

878   J., Miller, A. J., Minobe, S., Nakamura, H., Schneider, N., Vimont, D. J., Phillips, A. S.,

879   Scott, J. D., and Smith, C. A.: The Pacific decadal oscillation, revisited, J. Climate, 29,

880   4399–4427, https://doi.org/10.1175/ JCLI-D-15-0508.1, 2016.

881   O'Brien, J. P. and Deser, C.: Quantifying and understanding forced changes to unforced modes

882   of atmospheric circulation variability over the North Pacific in a coupled model large

883   ensemble, *J. Climate*, 36, 17-35, doi: https://doi.org/10.1175/JCLI-D-22-0101.1, 2023.

884   Olivarez, H. C., Lovenduski, N. S., Brady, R. X., Fay, A. R., Gehlen, M., Gregor, L.,

885   Landschützer, P., McKinley, G. A., McKinnon, K. A., and Munro, D. R.: Alternate

886   histories: Synthetic large ensembles of sea-air CO_2 flux, Global Biogeochem. Cy., 36,

887   e2021GB007174, https://doi.org/10.1029/2021GB007174, 2022.

888   Persad, G. G., and Caldeira, K.: Divergent global-scale temperature effects from identical

889   aerosols emitted in different regions. Nat. Commun., 9, 3289,

890   https://doi.org/10.1038/s41467- 018-05838-6, 2018.

891   Rodgers, K. B., Lee, S. -S., Rosenbloom, N., Timmermann, A., Danabasoglu, G., Deser, C.,

892   Edwards, J., Kim, J. -E., Simpson, I., Stein, K., Stuecker, M. F., Yamaguchi, R., Bodai, T.,

893   Chung, E. -S., Huang, L., Kim, W., Lamarque, J. -F., Lombardozzi, D., Wieder, W. R., and

894   Yeager, S. G.: Ubiquity of human-induced changes in climate variability. Earth Sys.

895   Dyn., 12, 1393–1411, https://doi.org/10.5194/esd-12-1393-2021, 2021.

896   Rohde, R., Muller, R., Jacobsen, R., Perlmutter, S., Rosenfeld, A., Wurtele, J., Curry, J.,

897   Wickham, C., and Mosher, S.: Berkeley Earth temperature averaging process, Geoinf.

898   Geostat. Overview, 1:2, https://doi.org/10.4172/2327-4581.1000103, 2013.

899 Santer, B., Fyfe, J. C., Solomon, S., Painter, J. F., Bonfils, C., Pallotta, G., and Zelinka, M. D.:

900   Quantifying stochastic uncertainty in detection time of human-caused climate signals, Proc.

901   Natl. Acad. Sci., 116, 19821–19827, https://doi.org/10.1073/pnas.1904586116, 2019.

902 Scaife, A. A., Arribas, A., Blockley, E., Brookshaw, A., Clark, R. T., Dunstone, N., Eade, R.,

903   Fereday, D., Folland, C. K., Gordon, M., Hermanson, L., Knight, J. R., Lea, D. J.,

904   MacLachlan, C., Maidens, A., Martin, M., Peterson, A. K., Smith, D., Vellinga, M.,

905   Wallace, E., Waters, J. and Williams, A: Skillful long-range prediction of European and

906   North American winters, Geophys. Res. Lett., 41, 2514–2519,

907   https://doi.org/10.1002/2014GL059637, 2014.

908 Scaife, A. A. and Smith, D.: A signal-to-noise paradox in climate science. Npj Clim. Atmos.

909   Sci., 1, 28 (2018), https://doi.org/10.1038/s41612-018-0038-4, 2018.

910 Schneider, D. P., Deser, C., and Fan, T.: Comparing the impacts of tropical SST variability and

911   polar stratospheric ozone loss on the Southern Ocean westerly winds, J. Climate, 28, 9350-

912   9372, https://doi.org/10.1175/JCLI-D-15-0090.1, 2015.

913 Schneider, U., Fuchs, T., Meyer-Christoffer, A., and Rudolf, B.: Global precipitation analysis

914   products of the GPCC. Global Precipitation Climatology Centre (GPCC), DWD, Internet

915   Publikation, 1-12.

916 Shepherd, T.: Atmospheric circulation as a source of uncertainty in climate change

917   projections, Nature Geosci., 7, 703–708 (2014), https://doi.org/10.1038/ngeo2253, 2014.

918 Sippel, S. Meinshausen, N., Merrifield, A., Lehner, F., Pendergrass, A. G., Fischer, E., and

919   Knutti, R.: Uncovering the forced climate response from a single ensemble member using

920   statistical learning, J. Climate, 32, 5677-5699, https://doi.org/10.1175/JCLI-D-18-0882.1,

921   2019.

922   Smith, D., Eade, R., Scaife, A. A., Caron, L. -P., Danabasoglu, G., DelSole, T. M., Delworth, T.,

923   Doblas-Reyes, F. J., Dunstone, N. J., Hermanson, L., Kharin, V., Kimoto, M., Merryfield,

924   W. J., Mochizuki, T., Müller, W. A., Pohlmann, H., Yeager, S., and Yang, X: Robust skill

925   of decadal climate predictions, Npj Clim. Atmos. Sci., 2, 13 (2019),

926   https://doi.org/10.1038/s41612-019-0071-y, 2019.

927   Smith, D. M. et al. North Atlantic Climate far more predictable than models imply, Nature, 583,

928   796–800, 2020.

929   Smith, D. M., Scaife, A. A., Eade, R., Athanasiadis, P., Bellucci, A., Bethke, I., Bilbao, R.,

930   Borchert, L. F., Caron, L.P., Counillon, F., Danabasoglu, G., Delworth, T., Doblas-Reyes,

931   F. J., Dunstone, N.J., Estella-Perez, V., Flavoni, S., Hermanson, L., Keenlyside, N., Kharin,

932   V., Kimoto, M., Merryfield, W. J., Mignot, J., Mochizuki, T., Modali, K., Monerie, P. A.,

933   Müller, W. A., Nicolí, D., Ortega, P., Pankatz, K., Pohlmann, H., Robson, J., Ruggieri, P.,

934   Sospedra-Alfonso, R., Swingedouw, D., Wang, Y., Wild, S., Yeager, S., Yang, X., and

935   Zhang, L.: North Atlantic climate far more predictable than models imply, Nature, 583,

936   796-800, https://doi.org/10.1038/s41586-020-2525-0, 2020.

937   Smoliak, B. V., Wallace, J. M., Lin, P., and Fu, Q.: Dynamical adjustment of the Northern

938   Hemisphere surface air temperature field: Methodology and application to observations, J.

939   Climate, 28, 1613–1629. https://doi.org/10.1175/JCLI-D-14-00111.1, 2015.

940   Stevenson, S., Fox-Kemper, B., Jochum, M., Neale, R., Deser, C., and Meehl, G.: Will there be

941   a significant change to El Nino in the 21st Century?, J. Climate, 25, 2129-2145,

942   https://doi.org/10.1175/JCLI-D-11-00252.1, 2012.

943 Strommen, K., Juricke, S., and Cooper, F.: Improved teleconnection between Arctic sea ice and

944   the North Atlantic Oscillation through stochastic process representation, Weather Clim.

945   Dynam., 3, 951–975, https://doi.org/10.5194/wcd-3-951-2022, 2022.

946 Suarez-Gutierrez, L., Milinski, S., and Maher, N.: Exploiting large ensembles for a better yet

947   simpler climate model evaluation, Clim. Dynam., 57, 2557–2580 (2021),

948   https://doi.org/10.1007/s00382-021-05821-w, 2021.

949 Swart, N. C., Fyfe, J. C., Hawkins, E., Kay, J. E., and Jahn A.: Influence of internal variability on

950   Arctic sea-ice trends. Nat. Clim. Change, 5, 86–89, https://doi.org/10.1038/nclimate2483,

951   2015.

952 Tebaldi, C., Dorheim, K., Wehner, M., Leung, R.: Extreme metrics from large ensembles:

953   investigating the effects of ensemble size on their estimates, Earth Syst. Dynam., 12 (4),

954   1427-1501, https://doi.org/10.5194/esd-12-1427-2021, 2021.

955 Tél, T., Bódai, T., Drótos, G., Haszpra, T., Herein, M., Kaszás, B., and Vincze, M.: The theory

956   of parallel climate realizations, J. Stat, Phys., 179, 1496–1530,

957   https://doi.org/10.1007/s10955-019-02445-7, 2020.

958 Terray, L.: A dynamical adjustment perspective on extreme event attribution, Weather Clim.

959   Dynam., 2, 971–989, https://doi.org/10.5194/wcd-2-971-2021, 2021.

960 Thompson, D. W. J., Barnes, E. A., Deser, C., Foust, W. E., and Phillips, A. S.: Quantifying the

961   role of internal climate variability in future climate trends, J. Climate, 28, 6443–6456,

962   https://doi.org/10.1175/JCLI-D-14-00830.1, 2015.

963 Trenary, L. and DelSole, T.: Does the Atlantic Multidecadal Oscillation Get Its Predictability

964   from the Atlantic Meridional Overturning Circulation?, J. Climate, 29, 5267-5280,

965   https://doi.org/10.1175/JCLI-D-16-0030.1, 2016.

966   Wallace, J.M., Deser, C., Smoliak, B. V., and Phillips, A. S.: Attribution of climate change in

967   the presence of internal variability, In Climate Change: Multidecadal and Beyond (Eds:

968   C.P. Chang, M. Ghil, M. Latif, and J. M. Wallace), World Scientific Series on Asia-Pacific

969   Weather and Climate, 6, 1-29, https://doi.org/10.1142/9789814579933_0001, 2013.

970   Wang, C., Deser, C., Yu, J. -Y., DiNezio, P., and Clement, A.: El Nino and Southern Oscillation

971   (ENSO): A Review. Coral Reefs of the Eastern Pacific, P. Glymn, D. Manzello and I.

972   Enochs, Eds., Springer Science Publisher, 4, 85-106, https://doi.org/10.1007/978-94-017-

973   7499-4_4, 2017.

974   Wills, R. C. J., Battisti, D. S., Armour, K. C., Schneider, T., and Deser, C.: Pattern recognition

975   methods to separate forced responses from internal variability in climate model ensembles

976   and observations, J. Climate, 33, 8693-8719, https://doi.org/10.1175/JCLI-D-19-0855.1,

977   2020.

978   Wittenberg, A. T.: Are historical records sufficient to constrain ENSO simulations?, Geophys.

979   Res. Lett., 36, L12702, https://doi.org/10.1029/2009GL038710, 2009.

980   Wu, X., Okumura, Y. M., Deser, C., and DiNezio, P. N.: Two-year dynamical predictions of

981   ENSO event duration during 1954–2015, *J. Climate*, 34(10), 4069-4087,

982   https://doi.org/10.1175/JCLI-D-20-0619.1, 2021.

983   Yeager, S. Danabasoglu, D., Rosenbloom, N. A., Strand, W., Bates, S. C., Meehl, G. A.,

984   Karspeck, A. R., Lindsay, K., Long, M. C., Teng, H., and Lovenduski, N. S.: Predicting

985   near-term changes in the Earth System: A large ensemble of initialized decadal prediction

986   simulations using the Community Earth System Model, *Bull. Am. Meteorol.* Soc. 99, 1867–

987   1886, https://doi.org/10.1175/BAMS-D-17-0098.1, 2018.

988   Zhang, R., Sutton, R., Danabasoglu, G., Kwon, Y.-O., Marsh, R., Yeager, S. G., Amrhein, D. E.,

989   and Little, C. M.: A review of the role of the Atlantic Meridional Overturning Circulation

990   in Atlantic Multidecadal Variability and associated climate impacts, Rev. Geophys., 57,

991   316–375, https://doi.org/10.1029/2019RG000644, 2019.